



HAL
open science

Tailored fluorinated oligo-polystyrene as efficient additive for the hydrophobicity/oleophobicity improvement of styrenic polymers

Ali Nourdine, Julien Giboz, Rachel Le Brouster, Florence Dubelley, Sylvain Carrier, Lionel Tenchine, Patrice Mele

► To cite this version:

Ali Nourdine, Julien Giboz, Rachel Le Brouster, Florence Dubelley, Sylvain Carrier, et al.. Tailored fluorinated oligo-polystyrene as efficient additive for the hydrophobicity/oleophobicity improvement of styrenic polymers. *European Polymer Journal*, 2021, pp.110712. 10.1016/j.eurpolymj.2021.110712 . hal-03328437

HAL Id: hal-03328437

<https://hal.science/hal-03328437>

Submitted on 16 Oct 2023

HAL is a multi-disciplinary open access archive for the deposit and dissemination of scientific research documents, whether they are published or not. The documents may come from teaching and research institutions in France or abroad, or from public or private research centers.

L'archive ouverte pluridisciplinaire **HAL**, est destinée au dépôt et à la diffusion de documents scientifiques de niveau recherche, publiés ou non, émanant des établissements d'enseignement et de recherche français ou étrangers, des laboratoires publics ou privés.



Distributed under a Creative Commons Attribution - NonCommercial 4.0 International License

Tailored fluorinated oligo-polystyrene as efficient additive for the hydrophobicity/oleophobicity improvement of styrenic polymers

A. Nourdine,^{1,*} J. Giboz,¹ R. Le Brouster,^{1,2} F. Dubelley,¹ S. Carrier,¹ L. Tenchine,² P. Mele¹

¹ Univ. Grenoble Alpes, Univ. Savoie Mont Blanc, CNRS, Grenoble INP*, LEPMI, 38000 Grenoble, France

* Institute of Engineering Univ. Grenoble Alpes

² IPC - Centre Technique Industriel de la Plasturgie et des Composites, Bellignat, France

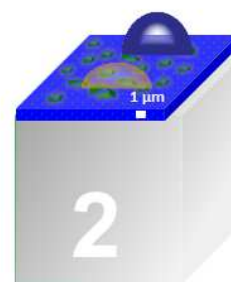
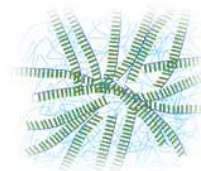
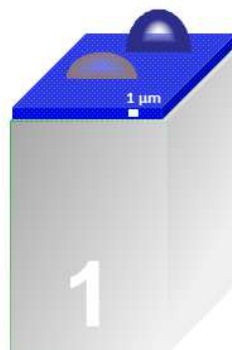
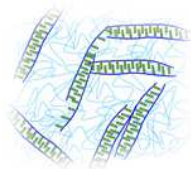
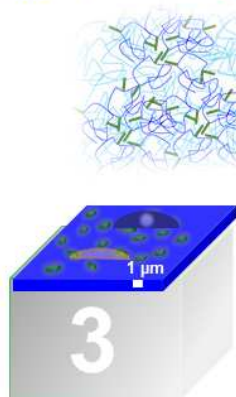
Keywords:

Hydrophobicity, oleophobicity, wettability, fluorinated additive, fluorine, polystyrene, polymerization

Summary

I.	Graphical abstract	3
II.	Abstract	4
III.	Introduction	5
IV.	Experimental section	6
IV.1.	Materials	6
IV.2.	Synthesized products and polymers:	6
IV.3.	Instrumental	8
V.	Results and discussions	10
V.1.	Synthesis of PS-type fluorinated additives	10
V.1.1.	Optimal synthesis route	10
V.1.2.	Chemical characterizations	12
V.1.3.	Morphological characterizations	18
V.1.3.1.	Analyses of the crystalline structures	18
V.1.3.2.	Thermal transitions	20
V.1.3.3.	Miscibility of PS and P[(S)_x-co-(S-MOM-C₉F₁₉)_y] blends	22
V.1.4.	Relationship molecular structure-microstructure-miscibility with PS	24
V.1.5.	Wettability characterizations	25
V.1.5.1.	Characterizations of the hydrophobicity	25
V.1.5.2.	Characterizations of oleophobicity	27
VI.	Conclusion	29
VII.	References	30

I. Graphical abstract



II. Abstract

The hydrophobic and oleophobic surface properties of polystyrene can be improved by using specific perfluorinated polystyrene copolymers as additives. In this work, an efficient synthetic route consisting in chemical modification via nucleophile substitution of chlorinated copolymers precursors was optimized. FTIR, $^1\text{H-NMR}$, $^{13}\text{C-NMR}$ and $^{19}\text{F-NMR}$ spectroscopic techniques were used to verify the overall conversion of reactions, characterize the chemical structures and quantify the composition of fluorinated part in the synthesized copolymers. Additionally, the thermal characterizations performed by Differential Scanning Calorimetry and the microstructure revealed by Optical Microscopy and X-ray diffraction, evidenced that the copolymer based on 19 mol.% of fluorinated monomer exhibits a singular properties and seems closer to a periodic copolymer conformation. These singular properties would originate from an interpenetrating conformation and explain the homogeneous morphology for all formulations based on this copolymer in comparison with copolymers based on 4 and 37 mol.% of fluorinated monomer. Finally, the functionality of the synthesized copolymers was evaluated, by measurement of water/oil static contact angles, and also in blend with a commercial polystyrene matrix at various wt.% of additives ranging from 100 ppm to 100 %. The effects of nature and content of copolymers on the hydrophobic and oleophobic surface properties were investigated. For all copolymers, the more the additive content increases, the more the surface properties are improved, obeying a threshold behavior for 4 and 37 mol.% and a quasi-linear behavior for 19 mol.%. Finally, it was evidenced that the surface properties improvement results both from the presence of a critical percentage of fluorine in the polymers blends and its consequence on the morphological properties. The additive based on 19 mol.% of fluorinated monomer allowing the achievement of higher static contact angles even with very low percentages of additive was identified as an optimal additive for improvement of polystyrene surface properties.

III. Introduction

Functionalization of polymer products via the chemical modification of the surface or by the integration of additives is an interesting industrial strategy to bring additional functionalities to products (e.g. self-cleaning/anti-fouling/anti-pollution,[1, 2] anti-fogging,[3] anti-corrosion,[4] antibacterial[5]...) for various applications such as energy,[1, 2] biomedical,[6] agro-alimentary,[7] transport industry,[8]...Bring or improve these functionalities imply the mastering of the intrinsic hydrophobic and oleophobic properties at molecular scale and surface topography/roughness at nano/microscale.[9-13] For the manufacturing of products with such properties, the existing industrial processes are mainly based on additional post-treatments or curing by i/ wet routes such as layer-by-layer and sol-gel techniques,[14] coating of solutions or inks [2, 4, 15] ii/ electrochemical or electrophoretic deposition [16, 17] iii/ plasma treatment.[14] or iv/ chemical or physical vapor deposition [14, 18]. The development of these processes is limited by economic, sustainability and ecological constraints, such as materials/process costs, low durability, eco-toxicity of inks or coatings and final recyclability of products.

An economically and efficient alternative solution to overcome these limitations could be the replacement of the coatings use by the development of new polymers materials based on commercial polymers with improved intrinsic surface properties. The wettability can then be modulated by incorporating low few hundred ppm of a mobile organic copolymer compatible with the commercial polymers.[19] These new polymeric systems could be potentially more efficient over time than usual commercial Polymer Processing Additives (PPA) (such as fatty acids, acid esters or acid amides), developed mainly for extrusion process aid and not for the final properties of injection molded/extruded products.[20, 21] The improvement of the processing and surface properties induced by these tailored copolymer could allow creation or improvement of commercial products with new functional properties while using the industrial existing processes including extrusion, injection molding or hot-embossing.[22]

The aim of this work is the development of efficient and specific surface agents for polystyrene, based on self-assemblable semi-fluorinated styrenic copolymers (hydrophobic-linked-superhydrophobic type) with various and controlled chemical compositions in order to find a good compromise between chemical compatibility with polystyrene, homogeneity of polymer/additive blends, optimal micro-nanostructures for maximizing the hydrophobic/oleophobic properties of styrenic polymers in static conditions.

IV. Experimental section

IV.1. Materials

The polymers used in this work are: polystyrene (PS) and fluorinated polystyrene copolymer poly(styrene-co-p-styrene-methyl-O-methyl-perfluorononyl) named P[(S)_x-co-(S-MOM-C₉F₁₉)_y]. The chemical structures are given in Scheme 1S. A commercial polystyrene with weight-average molar mass M_w close to 250 kg.mol⁻¹ and a Dispersity Index (PDI = M_w/M_n) of 2-2.3 was purchased from Total Petrochemical (reference PS 1160). A series of P[(S)_x-co-(S-MOM-C₉F₁₉)_y] were synthesized in laboratory as described below.

IV.2. Synthetized products and polymers

The grade pure solvents purchased from Carlo-Erba were used without prior purification. Monomers (styrene (S) and chloromethylstyrene (CMS)) purchased from Sigma Aldrich were purified by distillation before their uses. All air sensitive syntheses were carried out under dry nitrogen atmosphere using dried glassware.

- Synthesis of TEMPO-styrene: TEMPO-styrene was used as an initiator controller of both polymerization and copolymerization reactions (Scheme 1).[23] TEMPO-styrene was synthesized in laboratory from the nitroxide TEMPO• and 1-bromoethylbenzene using Atom Transfer Radical Addition (ATRA) method. In 50 mL two-necked round-bottom flask, the copper bromide CuBr (860 mg; 6 mmol) and the bipyridine ligand (860 mg; 6 mmol) are dissolved in anhydrous benzene (8 ml). The solution is degassed by bubbling nitrogen through for 10 minutes. In another 50 mL two-necked round-bottom flask, 1-bromoethylbenzene (1.12 g; 6 mmol) and the TEMPO• nitroxide radical (470 mg; 3 mmol) are dissolved in anhydrous benzene (8 ml). The second solution is degassed by bubbling nitrogen through for 10 minutes, then cannulated and added to the first. The reaction mixture is stirred at 60 °C under nitrogen for 5 hours. At the end of the reaction, 50 ml of diethylether are added to the reaction mixture. The precipitate obtained is filtered through Celite and the filtrate is extracted with 50 ml of a 5% wt/vol aqueous solution of CuSO₄ and then twice with 50 ml of water. The final solution is dried over MgSO₄ and concentrated by evaporation of the solvents under reduced pressure. The final product is purified on a silica chromatographic column. The chromatographic columns were carried out on silica gel60, particle size 0.063-0.2 mm with an eluent based on pentane/diethyl ether mixture (98/2). The final product are yellowish white crystals. ¹H-NMR (CDCl₃): 0.66 (1s; 3H ; CH₃) ; 1.03 (1s; 3H ; CH₃) ; 1.17 (1s; 3H ; CH₃) ; 1.37 (1s; 3H ;

CH₃); 1.29-1.48 (m; 6H ; CH₂); 1,47 (d; J= 6.7Hz ; 3H; CH₃); 4.77 (q; J= 6.7Hz; 1H; CH); 7.20-7.37 (m; 5H; CH_{aromatic}).

- Synthesis of P[(S)_x-co-(S-M-Cl)_y] copolymers precursors (Scheme 1): synthesis example of a target P[(S)₇₈-co-(S-M-Cl)₂₂]. In a two-necked flask, the TEMPO-Styrene initiator (0.26 g; 1 mmol) is added and degassed for 10 min. Then freshly distilled styrene (3.54 g; 34 mmol) and chloromethylstyrene (CMS) (or 4-vinylbenzyl chloride) (1.46 g; 9.58 mmol) are added and the mixture is degassed for 10 min refluxed at 130 °C for 10 hours under nitrogen. At the end of the reaction, the reaction mixture (viscous mixture) is cooled to room temperature, dissolved in CHCl₃, and then precipitated twice in methanol. After filtration, the polymer obtained (white powder) is dried under vacuum.

- Synthesis of P[(S)_x-co-(S-MOM-C₉F₁₉)_y] copolymers, i.e. functionalization chlorinated precursors P[(S)_x-co-(S-M-Cl)_y] (Scheme 1): synthesis example of a target P[(S)₇₈-co-(S-MOM-C₉F₁₉)₂₂]. In 50 ml flask, 1H,1H-Perfluoro-1-decanol (0.96 g; 1.91 mmol) (exceeding reagent) is added with 8 mL of a 25% aqueous solution of NaOH and stirred vigorously during 10 min. Then a solution containing Tetrabutylammonium hydroxide (TBAH, 40 wt.% in H₂O) (0.05 mL; 0.19 mmol) and 8 mL of CH₂Cl₂ is added and stirred vigorously during 10 min. Precursor copolymer P[(S)₇₈-co-(S-M-Cl)₂₂] (1 g; n(S-M-Cl) = 1.59 mmol) (limiting reagent) is added in the reactional medium and stirred for 18 hours at 40 °C. The excess of unreacted HO-CH₂-C₉F₁₉ was successfully removed during the purification. At the end of the reaction, the reaction medium is washed with HCl (0.1 M) until pH neutralization, then 3 times with distilled water. The neutral organic phase is dried over MgSO₄, filtered and concentrated, a white powder is obtained. After filtration, the polymer obtained (white powder) is dried under vacuum.

IV.3. Formulation route

Formulation route of PS/ P[(S)_x-co-(S-MOM-C₉F₁₉)_y]: polymers blends based on commercial PS and synthesized copolymers P[(S)₉₆-co-(S-MOM-C₉F₁₉)₄], P[(S)₈₁-co-(S-MOM-C₉F₁₉)₁₉] and P[(S)₆₃-co-(S-MOM-C₉F₁₉)₃₇] with fluorinated copolymer weight content ranging from 10⁻⁴ to 10¹ wt.% were elaborated (see table in Scheme 2S). As shown in Scheme 2S the formulation route consists in preparing two mother solutions: (1) 20 g/l of copolymers in acetone, (2) 20 g/l of polystyrene in dichloromethane. Then, various volumes of additive solutions were taken according to the target weight ratios and acetone was evaporated at ambient conditions during 24 hours. Dried additives were then re-dissolved in a volume of

polystyrene according to the target weight ratios PS/copolymer. Finally, the solutions were transferred to PTFE molds ($\phi = 73$ mm) and then the solvent was slowly evaporated at ambient conditions under confined atmosphere during 12 hours. Homogeneous films with controlled thickness (80-100 μm) were obtained.

I.1. Instrumental

I.1.1. Chemical analyses of additives

- Nuclear Magnetic Resonance (NMR) analyses: ^1H -NMR, ^{13}C -NMR and ^{19}F -NMR analyses were recorded using a Bruker Advance III 400 MHz/Ultrashield Plus Spectrometer System at ambient temperature in deuterated chloroform and/or acetone. Chemical shifts are expressed as (δ) and values are reported in parts per million (ppm).
- Fourier Transform InfraRed (FTIR) analyses: FTIR spectra performed in this work were collected in an attenuated total reflection mode on germanium crystal by Perkin Elmer Spectrum 400 series between 4000 and 600 cm^{-1} with a resolution of 2 cm^{-1} .
- Characterizations of molar masses and dispersity: Size Exclusion Chromatography (SEC) analyses were performed at ambient temperature (25 $^{\circ}\text{C}$) in tetrahydrofuran (THF). Number-average molar weight (M_n), weight average molar mass (M_w) and dispersity index ($\text{PDI} = M_w/M_n$) were estimated against polystyrene standards using a bank of 2 columns (WATERS Styragel HR4 + HR3) with THF eluting at a flow rate of 1.0 $\text{mL}\cdot\text{min}^{-1}$. Sample solutions were filtered through a 0.45 μm PTFE filter, and the detection chromatograph was controlled by WATERS 600 isocratic pump and connected to a refractometric detector (WATERS 2414).

I.1.2. Morphological analyses of additives and blends

- Characterizations of the crystalline phases: Wide-Angle X-Ray Diffraction patterns were obtained in reflection mode with a θ - θ diffractometer (X'Pert Pro MPD from PANalytical, CMTTC), with a rotating sample. The scan range was $3.96 < 2\theta < 60^{\circ}$ and the parameters were 45 kV and 40 mA for the X-rays copper (Cu) source, giving a Cu $K\alpha$ radiation with the corresponding wavelength $\lambda = 1.5419$ \AA . This allows a good compromise between the time for analysis and the peak-to-background ratio. The variations within the patterns due the amount of the fluorocopolymer $\text{P}[(\text{S})_x\text{-co-(S-MOM-C}_9\text{F}_{19})_y]$, the sample positioning, the reflection angle, the beam fluctuations are circumvented by normalizing the patterns in such a manner that the intensity underneath patterns is equal to unity. The plots give the intensity as a function of the d-spacing, calculated from the scattering angle and applying Bragg's law.

- Characterizations of thermal transitions: the thermal properties of synthesized oligo-polystyrene, oligo-copolymer, commercial polystyrene, formulated polymers blends and commercial fluorinated alcohol were quantified using a PerkinElmer Series 7 differential scanning calorimeter (DSC) at a heating or cooling rate of (+/-) 20 °C/min between 30 and 120 °C. The DSC instrument was calibrated with Indium ($T_{\text{onset}} = 156.6 \text{ °C}$, $\Delta H_{\text{fusion}} = 28.6 \text{ J/g}$) and Zinc ($T_{\text{onset}} = 419.47 \text{ °C}$) as calibration standards. Glass transition, melting and crystallization temperatures were determined from two heating and cooling cycles.

- Characterizations of the morphology: optical microscopy images were obtained using a LEICA-DM-LM microscope, a Leica DFC420 CCD camera and LEICA software in light transmission mode and with a 10x objective (magnification x100) to exhibit the surface morphology (a polarizer and an analyzer that is crossed with respect to the polarizer were used). These allow a qualitative comparison of the blends morphologies. A quantitative analysis was also conducted thanks to the *ImageJ* freeware and using the subsequent image processing steps: thresholding with a maxentropy filter, despeckle two times, and then analyzing the nodules surfaces and their numbers.

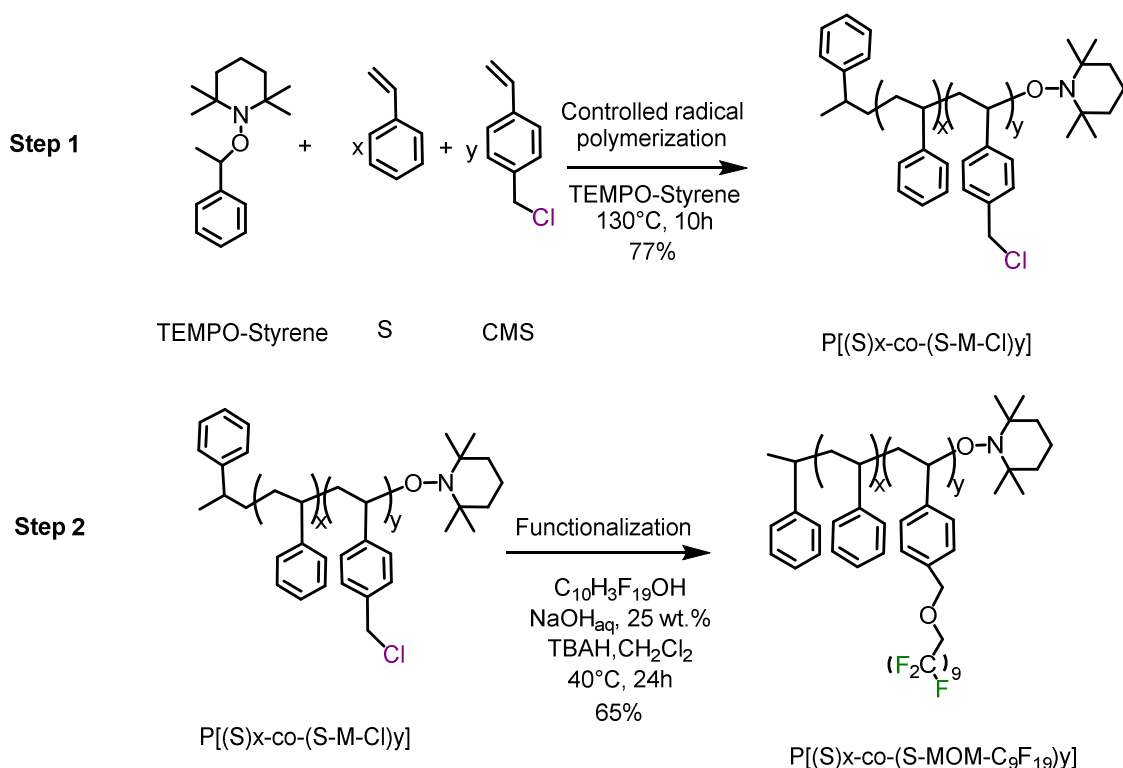
I.1.3. Wettability properties measurements

Static Contact Angle (CA) measurements were performed at room temperature on films (80-100 μm) using a DIGIDROP goniometer (GBX Instrument) equipped with a camera of resolution 718x452 pixels and the analysis software *Visiodrop*. The angles were estimated thanks to the Ultrapure water ($R > 10 \text{ M}\Omega\cdot\text{cm}$) used for hydrophilic properties characterizations and a commercial silicon oil (density of 0.91, $M_w = 900\text{-}1100 \text{ g/mol}$ and viscosity of 5 mPa.s) for oleophobic properties characterizations. Drops volume of 0.7 μl and a 5 s stabilization time were chosen as optimal conditions.

II. Results and discussions

II.1. Optimal synthesis of PS-type fluorinated additives

II.1.1. Synthesis route



Scheme 1. Synthetic schemes for $P[(S)_x\text{-co-}(S\text{-MOM-C}_9\text{F}_{19})_y]$

Several synthesis routes of fluorinated polymers are reported in literature,[24] e.g., polymer grafting,[25] coupling by nucleophilic substitution,[26] direct fluorination of polymers, polycondensation,[27] copolymerization of fluorinated monomers,[25, 28-31] and chemical modification of precursors polymers.[25, 32] In this work, copolymerization of fluorinated and non-fluorinated monomers (Scheme 3S) and chemical grafting of fluorinated chain onto polystyrene backbone (Scheme 1) were compared. The Table 1S summarizes the preliminary syntheses performed using the both synthesis routes. Several criteria including final synthesized polymers properties (molar mass, dispersity), controllability and yield of the reactions were considered to select the optimal synthesis route. Qualitatively, the functionalization of synthesized chlorinated polymer (i.e., route 2) seems more efficient and controllable than the functionalization of chlorinated monomer followed by its polymerization (i.e., route 1). Accordingly, the covalent grafting of fluorinated chain onto polystyrene precursor was chosen and successfully used to synthesize copolymers with various contents of fluorinated monomer at gram scale (Table 1).

Table 1. Chemical characteristics of the synthesized poly(styrene-co-p-styrene-methyl-O-methyl-perfluorononyl) P[(S)-co-(S-MOM-C₉F₁₉)_y] copolymers

Polymers	Effective mol.% y ^a	M _n g/mol ^b	M _w g/mol ^b	PDI	Number total of monomers/chain	Number of monomer S/ chain	Number of monomer S-MOM-C ₉ F ₁₉ /chain
P[(S) ₉₆ -co-(S-MOM-C ₉ F ₁₉) ₄]	3,4	4900	5500	1,12	47	45-46	1-2
P[(S) ₈₁ -co-(S-MOM-C ₉ F ₁₉) ₁₉]	19	5340	6530	1,22	51	41-42	9-10
P[(S) ₆₃ -co-(S-MOM-C ₉ F ₁₉) ₃₇]	36,8	5700	7500	1,32	55	34-35	20-21

The nomenclature adopted is P[(S)_x-co-(S-MOM-C₉F₁₉)_y]; where y is the molar fraction of monomer S-MOM-C₉F₁₉

^a Determined by ¹H-NMR spectroscopy in CDCl₃

^b Number-average (M_n), weight-average (M_w) molar masses and dispersity indices (M_w/M_n, PDI) were determined by SEC in THF on initial polymers precursors.

A series of copolymers containing 3.4, 19 and 36.8 mol.% of fluorinated monomer (S-MOM-C₉F₁₉) were synthesized via route 2 (Scheme 3S). The ex-situ reaction monitoring was carried out by spectroscopic techniques (IR, ¹H-NMR, ¹³C-NMR, ¹⁹F-NMR). The mol.% of S-MOM-C₉F₁₉ in final copolymers were quantified by ¹H-NMR from the ratio between aryl (4.5 ppm) or aliphatic (1-2 ppm) protons number.[33]

II.1.2. Chemical characterizations

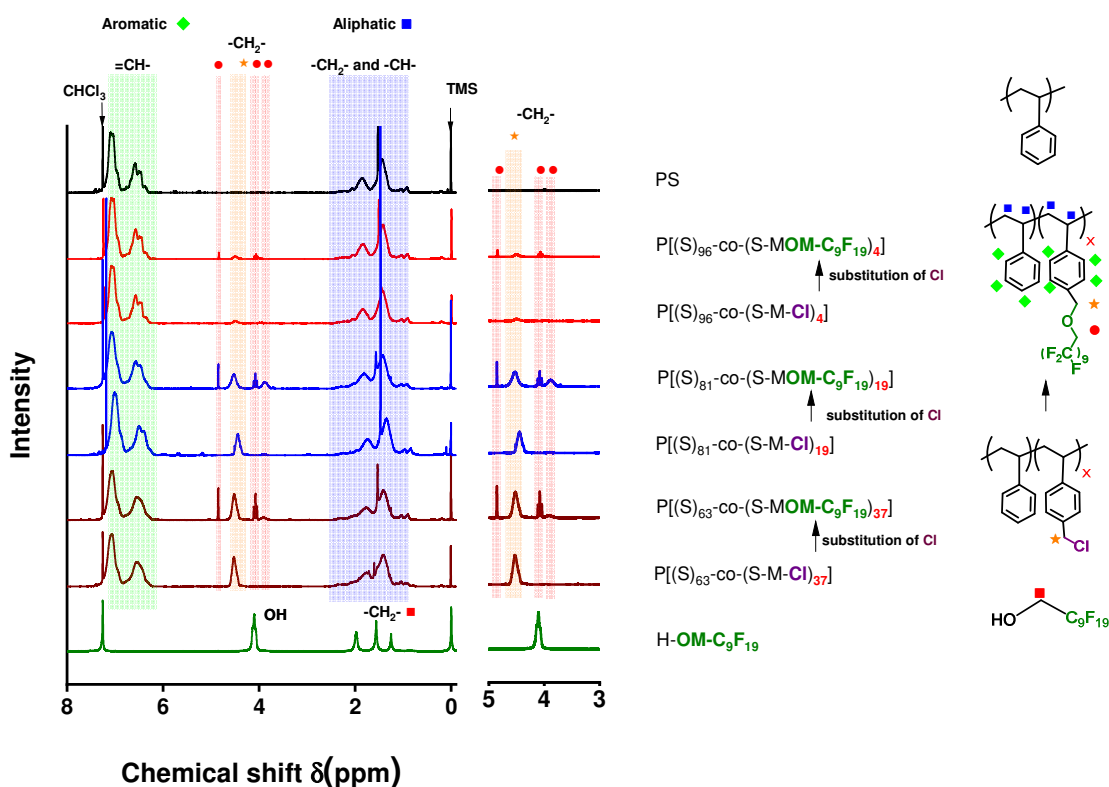


Figure 1. $^1\text{H-NMR}$ spectra of $P[(S)_{96}\text{-co-}(S\text{-MOM-C}_9\text{F}_{19})_4]$, $P[(S)_{81}\text{-co-}(S\text{-MOM-C}_9\text{F}_{19})_{19}]$ and $P[(S)_{63}\text{-co-}(S\text{-MOM-C}_9\text{F}_{19})_{37}]$ and their precursors $P[(S)_{96}\text{-co-}(S\text{-MOM-Cl})_4]$, $P[(S)_{81}\text{-co-}(S\text{-MOM-Cl})_{19}]$ and, $P[(S)_{63}\text{-co-}(S\text{-MOM-Cl})_{37}]$, respectively. PS and OH-CH₂-C₉F₁₉ are given for comparison and control.

Qualitatively, the overall conversions of functional groups were achieved (Figure 1). The appearance of new peaks at 4.85, 4.08 and 3.87 ppm whose intensities are correlated with mol.% of the grafted fluorinated chain except for the peak at 3.87 ppm which is relatively more intense for $P[(S)_{81}\text{-co-}(S\text{-MOM-C}_9\text{F}_{19})_{19}]$ confirms the success of total functionalization. These specific peaks differ from those of precursor polymer and those of fluorinated alcohol indicate an effective and total grafting of fluorinated chain onto polystyrene.

Additionally, For a given polymer, different chemical shifts for -CH₂- protons derived from the fluorinated graft despite being in the same positions in the chemical structure with a total number of 2 (Figure 1). This difference could be explained by both i/ the dissymmetric structure which induces a significant difference on the electronic environment (non-equivalent protons) and ii/ the molecular arrangement (inter and intramolecular interactions even in solution [34-37]) depending on the composition of the mol.% of -CH₂-C₉F₁₉: for example the peak at 3.87 ppm is relatively more intense for $P[(S)_{81}\text{-co-}(S\text{-MOM-C}_9\text{F}_{19})_{19}]$, less intense for

$P[(S)_{63}\text{-co-(S-MOM-C}_9\text{F}_{19})_{37}]$ and inexistent for $P[(S)_{96}\text{-co-(S-MOM-C}_9\text{F}_{19})_4]$. These hypotheses were investigated by $^{19}\text{F-NMR}$ (Figure 2) and $^{13}\text{C-NMR}$ (Figure 3).

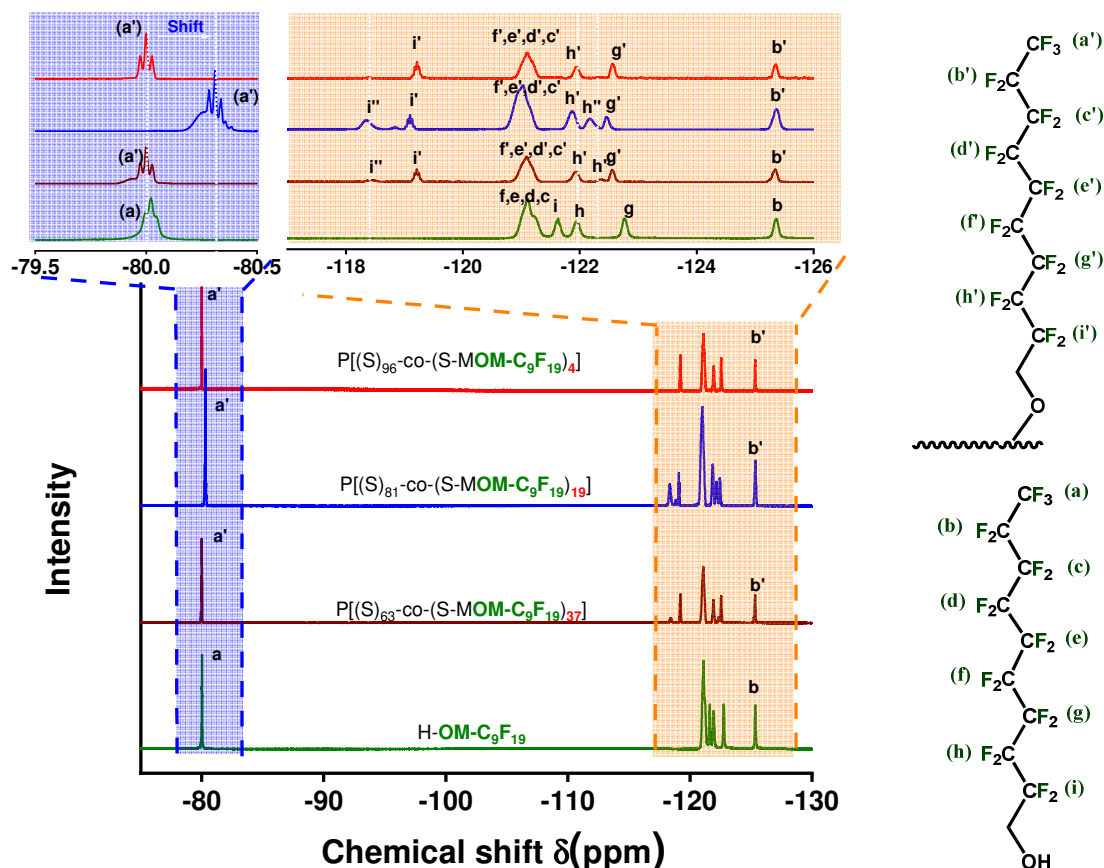


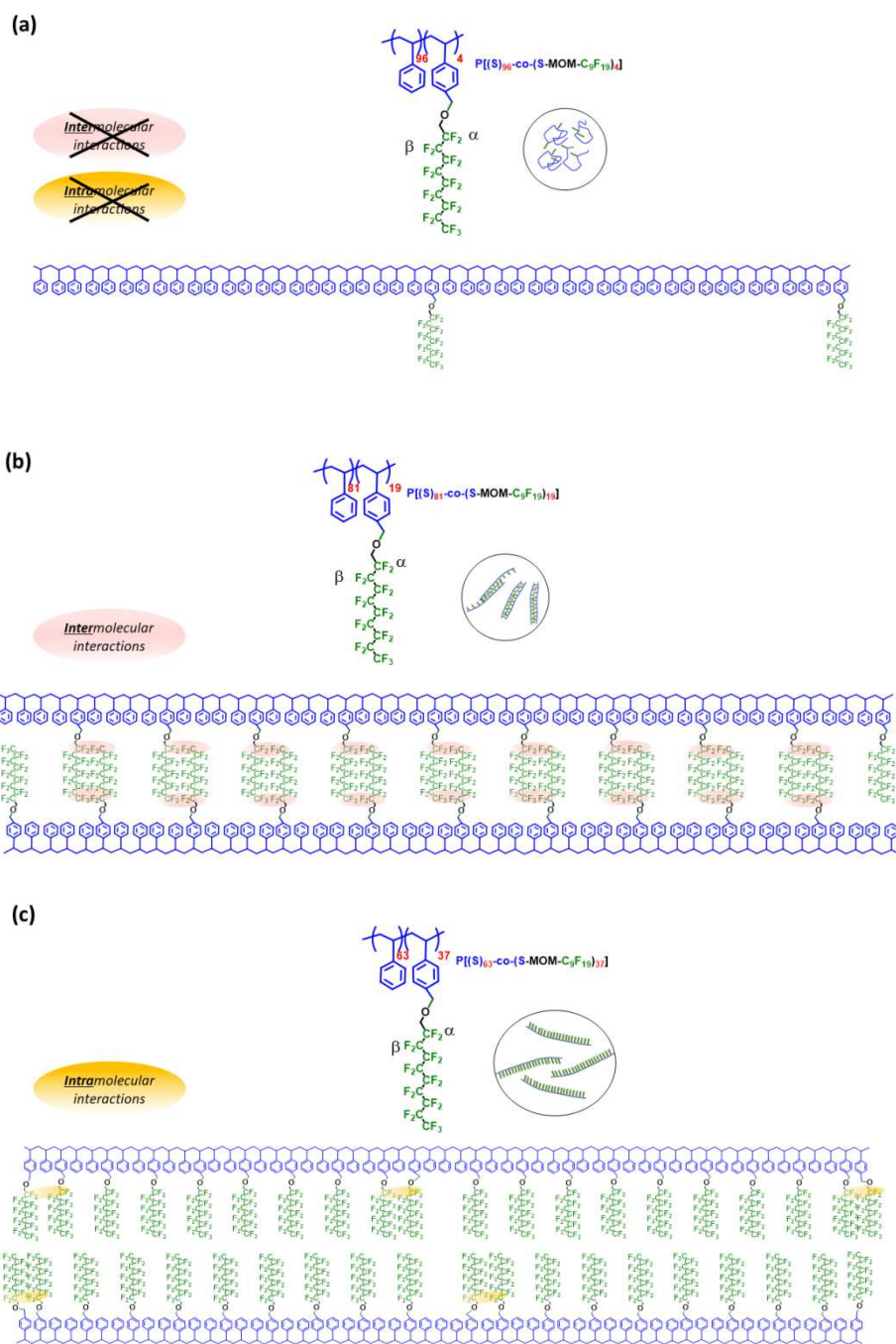
Figure 2. $^{19}\text{F-NMR}$ spectra of $P[(S)_{96}\text{-co-(S-MOM-C}_9\text{F}_{19})_4]$, $P[(S)_{81}\text{-co-(S-MOM-C}_9\text{F}_{19})_{19}]$ and, $P[(S)_{63}\text{-co-(S-MOM-C}_9\text{F}_{19})_{37}]$

The $^{19}\text{F-NMR}$ spectra in Figure 2 highlight the appearance of new $-\text{C-F}$ signals, totally different of those of $\text{HO-CH}_2\text{-C}_9\text{F}_{19}$. This is in accordance with IR analyses (Figure 4) and validates the total substitution of chloride in precursor polymer by fluorinated graft. Here also it can be observed a particular difference on $P[(S)_{81}\text{-co-(S-MOM-C}_9\text{F}_{19})_{19}]$ spectrum, compared to $P[(S)_{63}\text{-co-(S-MOM-C}_9\text{F}_{19})_{37}]$ and $P[(S)_{96}\text{-co-(S-MOM-C}_9\text{F}_{19})_4]$, with:

- i/ a shift of $-\text{CF}_3$ signal (peak a') at -80.3 ppm instead of -80 ppm
- ii/ $-\text{CF}_2-$ signals (peak i'') in α position of ether function ($-\text{O-CH}_2\text{-CF}_2\text{-...}$) are partly shifted towards the highest chemical values (from -119.1 ppm for (i') to -118.4 ppm for (i''))
- iii/ The peak (i'') seems to be non-correlated to the mol.% of $\text{S-MOM-C}_9\text{F}_{19}$ because is absent for $P[(S)_{96}\text{-co-(S-MOM-C}_9\text{F}_{19})_4]$, slightly present for $P[(S)_{63}\text{-co-(S-MOM-C}_9\text{F}_{19})_{37}]$ and significant for $P[(S)_{81}\text{-co-(S-MOM-C}_9\text{F}_{19})_{19}]$.

iv\ -CF₂- signals (peak h'') in β position of ether function (-O-CH₂-CF₂-CF₂-...) are partly shifted to the lowest chemical values from -121.9 ppm (h') to -122.2 ppm (h''). This shift is not observed for P[(S)_{96-co}-(S-MOM-C₉F₁₉)₄], slightly present for P[(S)_{63-co}-(S-MOM-C₉F₁₉)₃₇] and significant for P[(S)_{81-co}-(S-MOM-C₉F₁₉)₁₉].

¹⁹F-NMR spectrum of P[(S)_{81-co}-(S-MOM-C₉F₁₉)₁₉] evidenced distinguished signals, especially, -CF₃ signal (peak a'), -O-CH₂-CF₂-...signal (peak i'') and -O-CH₂-CF₂-CF₂-...CF₂- signals (peak h''). This is in accordance with the previous ¹H-NMR analysis and the appearance of -CH₂ protons (...O-CH₂-CF₂-...) in three positions at 4.85, 4.08 and 3.87 ppm (Figure 1). These noticeable differences for P[(S)_{81-co}-(S-MOM-C₉F₁₉)₁₉] in comparison with P[(S)_{96-co}-(S-MOM-C₉F₁₉)₄] and P[(S)_{63-co}-(S-MOM-C₉F₁₉)₃₇] are not linked to mol.% of -CH₂-C₉F₁₉ but to the intermolecular or intramolecular interactions (Scheme 2). P[(S)_{63-co}-(S-MOM-C₉F₁₉)₃₇] richer in fluorine than P[(S)_{81-co}-(S-MOM-C₉F₁₉)₁₉] would imply potentially more and stronger inter/intramolecular interactions but its conformation and the distribution of fluorinated chains along the PS backbone would counterbalance these interactions (Scheme 2). These differences at the molecular scale evidenced in the diluted system could also appear in undiluted conditions, at a solid state, and resulting properties could be affected. The morphology at the solid state and the thermal properties are then studied with Wide Angle X-ray Diffraction (WAXD), Optical Microscopy (OM) and Differential Scanning Calorimetry (DSC).



Scheme 2. Schemes of plausible molecular interactions (a) $P[(S)_{96}\text{-co-}(S\text{-MOM-C}_9\text{F}_{19})_4]$ (b) $P[(S)_{81}\text{-co-}(S\text{-MOM-C}_9\text{F}_{19})_{19}]$ (c) $P[(S)_{63}\text{-co-}(S\text{-MOM-C}_9\text{F}_{19})_{37}]$

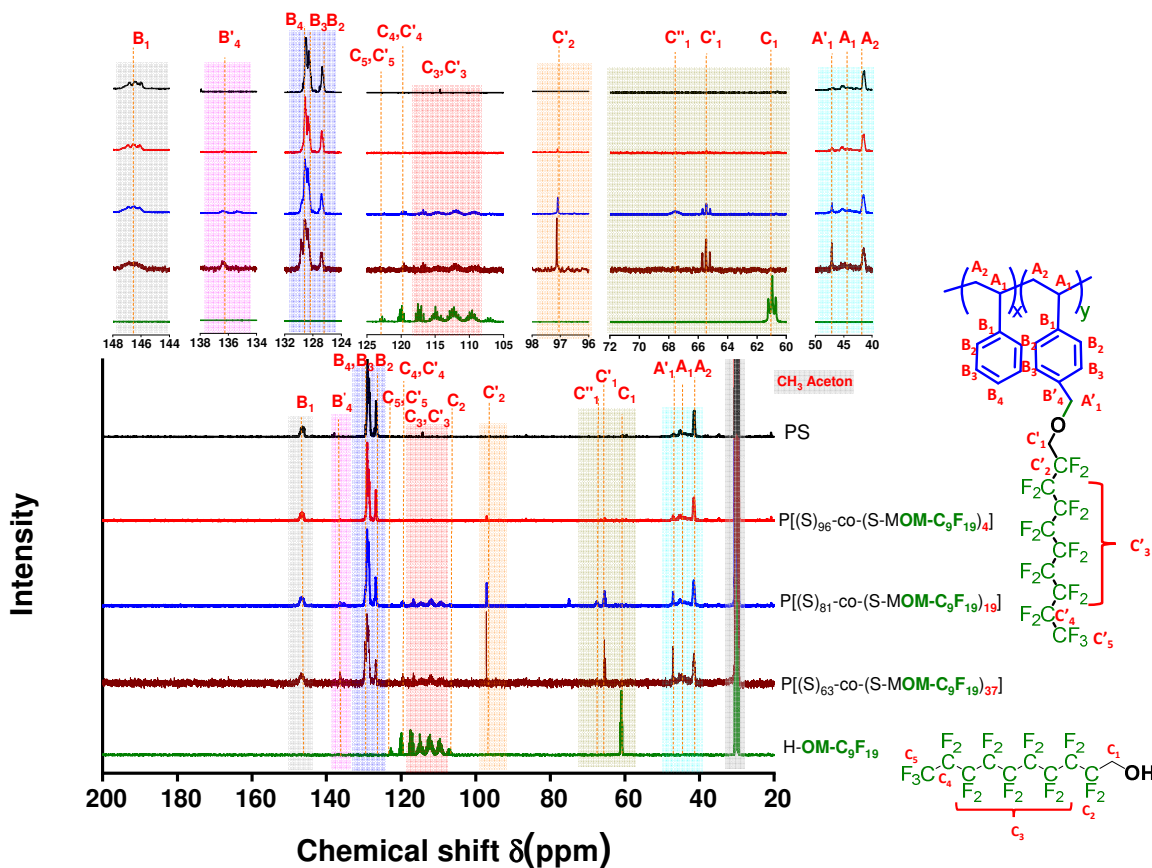


Figure 3. ^{13}C -NMR spectra of $P[(S)_{96}\text{-co-(S-MOM-C}_9\text{F}_{19})_4]$, $P[(S)_{81}\text{-co-(S-MOM-C}_9\text{F}_{19})_{19}]$ and $P[(S)_{63}\text{-co-(S-MOM-C}_9\text{F}_{19})_{37}]$ and their precursors $P[(S)_{96}\text{-co-(S-MOM-Cl)}_4]$, $P[(S)_{81}\text{-co-(S-MOM-Cl)}_{19}]$ and $P[(S)_{63}\text{-co-(S-MOM-Cl)}_{37}]$, respectively. PS and $\text{OH-CH}_2\text{-C}_9\text{F}_{19}$ are given for comparison and control of the synthesized products.

^{13}C -NMR spectroscopy was used as a complementary analysis. Figure 3 shows ^{13}C -NMR spectra of the synthesized copolymers and controls based on polystyrene and fluorinated alcohol $\text{HO-CH}_2\text{-C}_9\text{F}_{19}$. In agreement with ^1H -NMR (Figure 1), ^{19}F -NMR (Figure 2) and IR (Figure 4), ^{13}C -NMR (Figure 3) confirms also a complete conversion of functionalization reaction. As it can be seen, a signal of carbon in α position of hydroxyl function $\text{HO-CH}_2\text{-C}_9\text{F}_{19}$ (peak C'_1 at 60.96 ppm) in fluorinated alcohol disappears and after functionalization a new signal appears at 65.4 ppm which corresponds to carbon in α position of ether $\text{...-CH}_2\text{-O-CH}_2\text{-...}$ (triplet at 65.44 ppm). In comparison with $P[(S)_{96}\text{-co-(S-MOM-C}_9\text{F}_{19})_4]$ and $P[(S)_{63}\text{-co-(S-MOM-C}_9\text{F}_{19})_{37}]$, it can be observed a presence of an additional signal at 67.6 ppm which could result from a partial shift of the signal C'_1 (65.4 ppm) induced by the favorable inter/intramolecular interactions[36, 38] (Scheme 2).

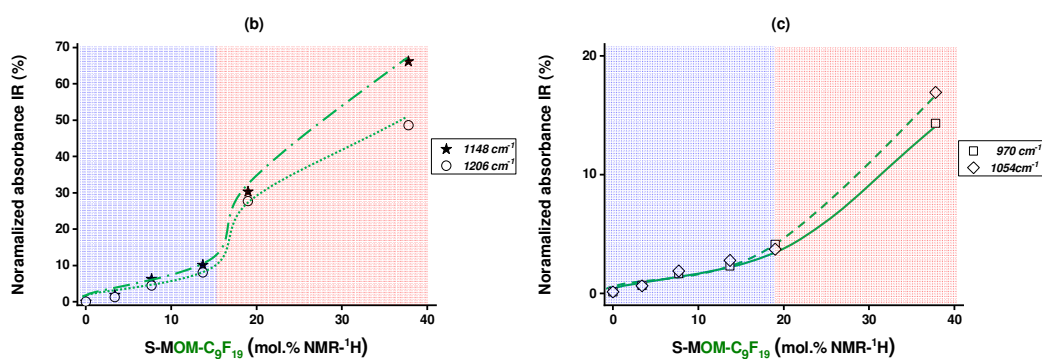
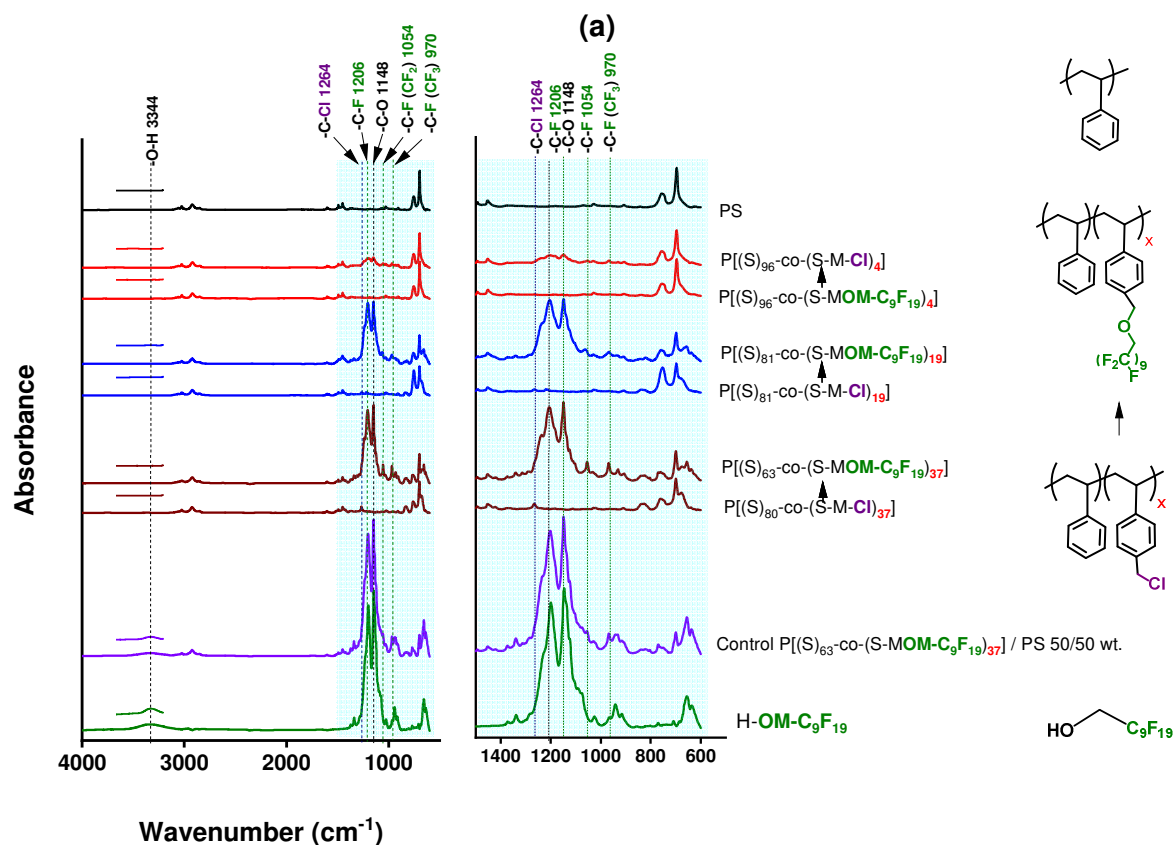


Figure 4. (a) FTIR spectra of $P[(S)_{96}\text{-co-(S-MOM-C}_9\text{F}_{19})_4]$, $P[(S)_{81}\text{-co-(S-MOM-C}_9\text{F}_{19})_{19}]$ and $P[(S)_{63}\text{-co-(S-MOM-C}_9\text{F}_{19})_{37}]$ and their precursors $P[(S)_{96}\text{-co-(S-MOM-Cl)}_4]$, $P[(S)_{81}\text{-co-(S-MOM-Cl)}_{19}]$ and $P[(S)_{63}\text{-co-(S-MOM-Cl)}_{37}]$, respectively. PS and OH-CH₂-C₉F₁₉ are given for comparison and control. (b) Normalized IR absorbance intensity versus MOM-C₉F₁₉ composition in $P[(S)_x\text{-co-(S-MOM-C}_9\text{F}_{19})_y]$ at 970 and 1054 cm⁻¹ (c) Normalized IR absorbance intensity versus MOM-C₉F₁₉ composition in $P[(S)_x\text{-co-(S-MOM-C}_9\text{F}_{19})_y]$ at 1148 and 1206 cm⁻¹. (Normalization used: 1% for the peak at 2922 cm⁻¹)

Figure 4(a) shows IR spectra of the three selected copolymers $P[(S)_{96}\text{-co-(S-MOM-C}_9\text{F}_{19})_4]$, $P[(S)_{81}\text{-co-(S-MOM-C}_9\text{F}_{19})_{19}]$ and $P[(S)_{63}\text{-co-(S-MOM-C}_9\text{F}_{19})_{37}]$ and their chlorinated precursors copolymers. Polystyrene, fluorinated alcohol HO-CH₂-C₉F₁₉ and physical blend $P[(S)_{63}\text{-co-(S-MOM-C}_9\text{F}_{19})_{37}]/\text{PS}$ 50/50 are used as controls. All IR spectra

evidenced a disappearance of hydroxyl band (3344 cm^{-1}), the appearance of ether function corresponding to the -C-O-C- bond (band at 1148 cm^{-1}) and -C-F bonds of -CF₂- and -CF₃ functions (bands at 970 , 1054 and 1206 cm^{-1}). These new signals seem correlated to mol.% of -CH₂-C₉F₁₉. Figure 4(b) shows the intensities of the bands at 970 , 1054 , 1148 and 1206 cm^{-1} versus the mol.% of -CH₂-C₉F₁₉. Therefore, the intensities of these bands increases with the mol.% of -CH₂-C₉F₁₉ in copolymer. A bimodal law was moreover evidenced. The bands intensities increase gradually and linearly for low mol.% of -CH₂-C₉F₁₉ (blue zone in Figure 4(b)) and non-linearly for higher mol.% of -CH₂-C₉F₁₉ (red zone in Figure 4(b)). This S-shape trend and the amplification of signals intensities for high mol.% of -CH₂-C₉F₁₉ reveal a presence of numerous and stronger inter/intramolecular interactions between the fluorinated segments and confirm the previous hypotheses (Scheme 2) developed from ¹H-NMR (Figure 1), ¹⁹F-NMR (Figure 2) and ¹³C-NMR (Figure 3).

II.1.3. Morphological characterizations

II.1.3.1. Analyses of the crystalline structures

From the previous chemical analyses in diluted conditions or at the solid state, it was assumed that specific and strong intermolecular interactions between fluorinated segments occur between the side chains. As the fluorine alcohol exhibits a crystalline behavior, the crystalline conformation of the different copolymers has been analyzed thanks to WAXD analysis. The diffraction patterns are given in Figure 5 for the different copolymers: the amorphous polystyrene and the fluorinated alcohol diffraction patterns are also superimposed as references. One can see the typical pattern of the amorphous polystyrene presenting two broad peaks corresponding to a d-spacing of 4.6 \AA and 9 \AA respectively.[39] In comparison, the copolymers show additional diffraction peaks.

Most of them are commonly found for the three copolymers @ 4.5 , 4.8 or 4.9 , 5.2 , 6.8 and 13 \AA . For the lowest d-spacing values, the peaks originate from the diffraction planes of the hexagonal packing of the fluoralkyl segments, the most intense @ 4.8 or 4.9 \AA corresponds to the reflection of the (100) plane, which is close to the intermolecular distance of the PTFE crystal,[39] as schemed in Scheme 3(a).

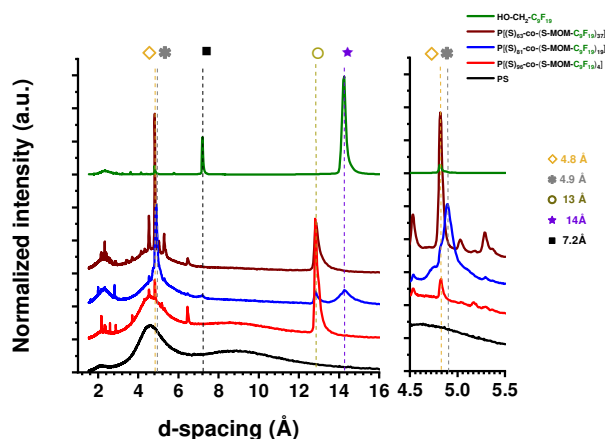
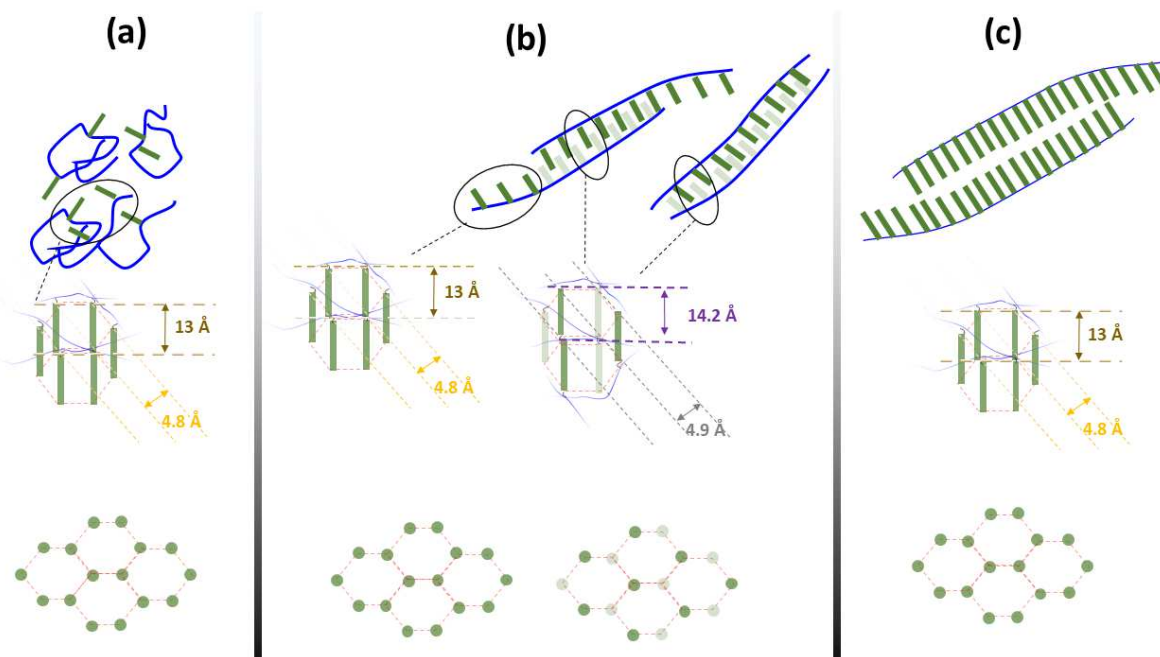


Figure 5. X-ray diffraction patterns representing the d-spacing for $P[(S)_{96}\text{-co-(S-MOM-C}_9\text{F}_{19})_4]$, $P[(S)_{81}\text{-co-(S-MOM-C}_9\text{F}_{19})_{19}]$ and $P[(S)_{63}\text{-co-(S-MOM-C}_9\text{F}_{19})_{37}]$, PS and $\text{OH-CH}_2\text{-C}_9\text{F}_{19}$ (given for comparison) (left: whole pattern; right: detailed view)

The peak @13 Å is related to a lamellar periodicity due to the stacking of the fluoroalkyl groups,[40] as schemed in Scheme 3. In the case of $P[(S)_{81}\text{-co-(S-MOM-C}_9\text{F}_{19})_{19}]$, the specific interactions previously evidenced involve some differences over the WAXD pattern for this copolymer. Indeed, on one hand the footprints between 2 and 3 Å are different, and on the other hand, a shift from 4.8 to 5 Å is observed together with a disappearance of the peak at 6.6 Å linked probably to distortions within the hexagonal packing and the lamellar stacking. Moreover, an additional high intensity peak @14.2 Å is observed together with a lower intensity one @7.2 Å. These peaks are precisely equivalent to the ones observed for the fluorinated alcohol, meaning that the structure adopted by the fluoroalkyl segments in this specific copolymer is the same than the one in alcohol. In this case, the groups conformation after crystallization seems then lowly affected by the polymer backbone, and mostly guided by intermolecular interactions between segments, at the manner of an interpenetrated morphology (Scheme 3), as observed by in the literature for fluorinated and non fluorinated copolymers.[37, 41-46]



Scheme 3. Schemes of the different crystalline structure existing in (a) P[(S)₉₆-co-(S-MOM-C₉F₁₉)₄], (b) P[(S)₈₁-co-(S-MOM-C₉F₁₉)₁₉] and (c) P[(S)₆₃-co-(S-MOM-C₉F₁₉)₃₇]

II.1.3.2. Thermal transitions

The relationship between fluorine content (*i.e.* functionalization degree) and resulting microstructure was investigated. Thermal transitions were analyzed by Differential Scanning Calorimetry (DSC), giving the thermograms in Figure 6 (a), (b) and (c) and Figure 6 (a'), (b') and (c') showing the second heating and cooling cycles, respectively. Glass transition temperature around 105 ± 1 °C and melting temperature close to 89 ± 1 °C were measured for the controls, *i.e.*, commercial polystyrene and fluorinated alcohol HO-CH₂-C₉F₁₉, respectively. All P[(S)_x-co-(S-MOM-C₉F₁₉)_y] copolymers exhibit a semi-crystalline behaviour with melting and crystallization temperatures. In the considered temperature range, no glass transition temperature (T_g) was detected for P[(S)₈₁-co-(S-MOM-C₉F₁₉)₁₉] and P[(S)₆₃-co-(S-MOM-C₉F₁₉)₃₇]. In contrast, P[(S)₈₁-co-(S-MOM-C₉F₁₉)₄] shows a glass transition temperature (105 ± 1 °C) related to the molecular mobility of PS backbone in P[(S)₉₆-co-(S-MOM-C₉F₁₉)₄]. It can be noticed also that P[(S)₈₁-co-(S-MOM-C₉F₁₉)₄] and P[(S)₈₁-co-(S-MOM-C₉F₁₉)₃₇] show a single crystallization temperature T_c at 61 ± 1 °C and a double melting temperature (T_m^1 and T_m^2) of fluorinated crystalline entities at 39 ± 1 and 72 ± 1 °C, respectively. In contrast, P[(S)₈₁-co-(S-MOM-C₉F₁₉)₁₉] exhibits a single crystallization

temperature at lower temperature (58 ± 1 °C) and a single melting temperature of fluorinated (71 ± 1 °C). This assumed a more homogeneous molecular arrangement and monodisperse crystallites sizes in this latter copolymer.

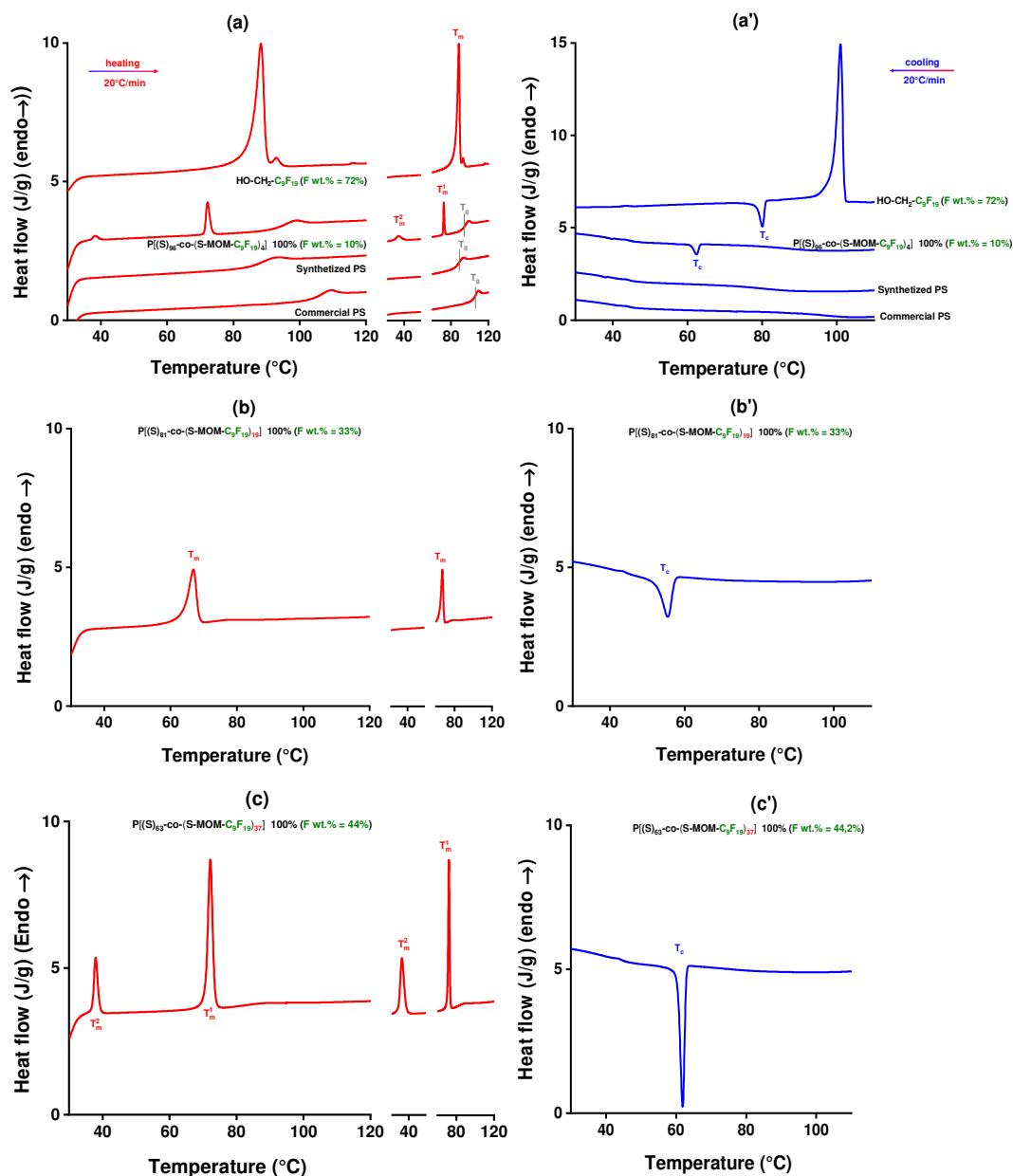


Figure 6. DSC traces of the second heating cycles of (a) $P[(S)_{96}\text{-co-(S-MOM-C}_9\text{F}_{19})_4]$ (b) $P[(S)_{81}\text{-co-(S-MOM-C}_9\text{F}_{19})_{19}]$ (c) $P[(S)_{63}\text{-co-(S-MOM-C}_9\text{F}_{19})_{37}]$. DSC traces of the second cooling cycles of (a') $P[(S)_{96}\text{-co-(S-MOM-C}_9\text{F}_{19})_4]$ (b') $P[(S)_{81}\text{-co-(S-MOM-C}_9\text{F}_{19})_{19}]$ (c') $P[(S)_{63}\text{-co-(S-MOM-C}_9\text{F}_{19})_{37}]$. DSC traces of pure PS and OH-CH₂-C₉F₁₉ are given in (a' and a'') for comparison. (heating and cooling rate = 20°C/min)

The crystallinity degrees of $P[(S)_x\text{-co-(S-MOM-C}_9\text{F}_{19})_y]$ copolymers were calculated using the ratio between the melting enthalpy at 72 °C and the melting enthalpy of fluorinated

alcohol HO-CH₂-C₉F₁₉. Figure 7 shows the evolution of crystallinity degree as function of fluorine weight content. The higher the fluorine content, the higher is the crystallinity degree. The trend seems to be quasi-linear, excepting for P[(S)₈₁-co-(S-MOM-C₉F₁₉)₁₉] sample, showing a higher crystallinity than P[(S)₆₃-co-(S-MOM-C₉F₁₉)₃₇], whereas it is richer in fluorine. This amplified crystallinity of P[(S)₈₁-co-(S-MOM-C₉F₁₉)₁₉] could be also related to the particular molecular interactions of this copolymer. This result is in accordance with the presence of a specific and strong molecular interactions previously evidenced by NMR and X-ray diffraction analysis.

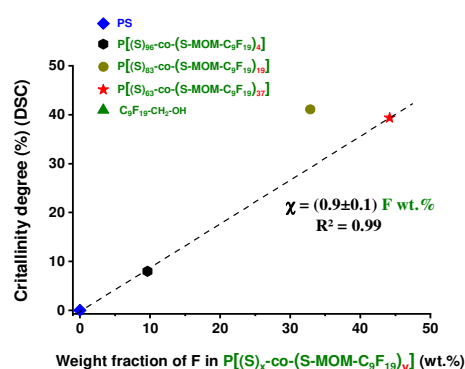


Figure 7. Crystallinity degree versus weight fraction of fluorine in $P[(S)_x\text{-co-(S-MOM-C}_9\text{F}_{19})_y]$ (crystallinity degree was calculated using fusion enthalpy measured in the second heating step and $\Delta H_0^{\text{HO-CH}_2\text{-C}_9\text{F}_{19}} = 38 \text{ J/g}$)

II.1.3.3. Miscibility of PS and $P[(S)_x\text{-co-(S-MOM-C}_9\text{F}_{19})_y]$ blends

It is now of interest to investigate the miscibility of $P[(S)_x\text{-co-(S-MOM-C}_9\text{F}_{19})_y]$ copolymers with a commercial PS, to use it as an additive. Qualitatively, the optical microscopy images shown in Figure 8 evidence the presence of birefringent heterogeneities related to the crystalline phases of fluorinated graft.

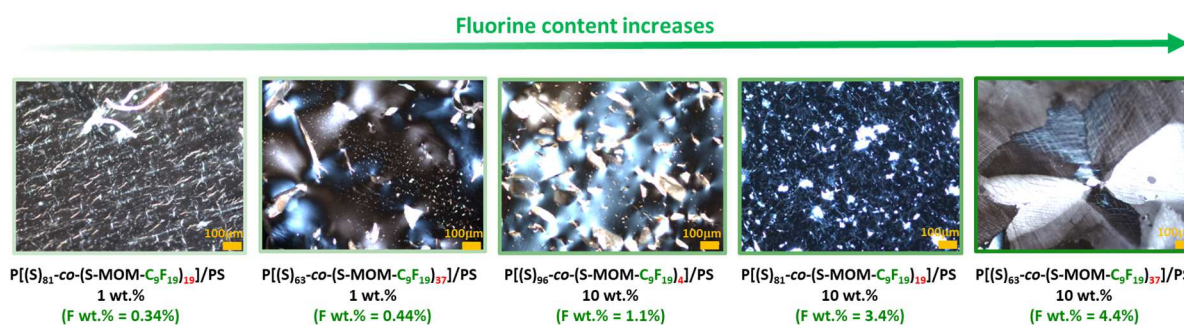
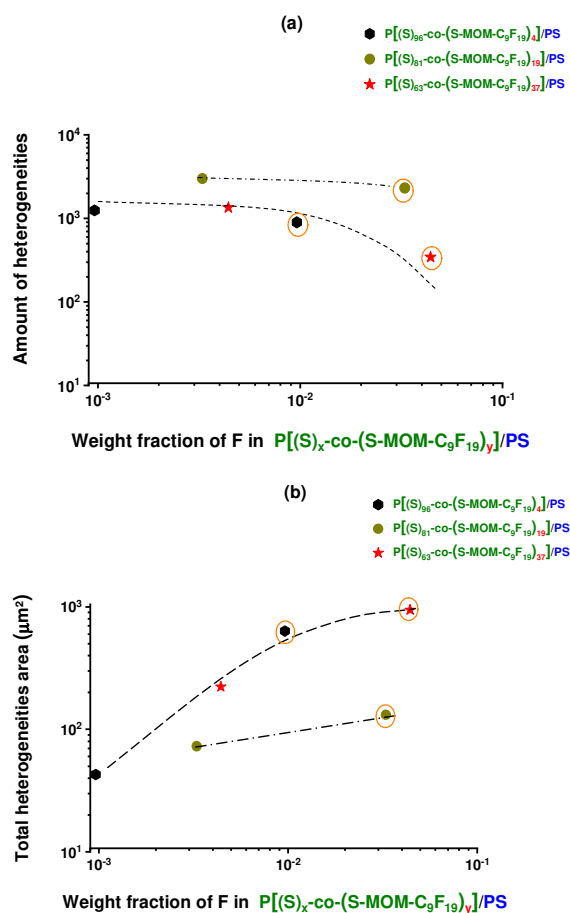


Figure 8. Optical microscopy images for various weight fraction of fluorine in $P[(S)_x\text{-co-(S-MOM-C}_9\text{F}_{19})_y]/\text{PS}$ blends

Quantitatively, depending on the fluorine content, the heterogeneities number (Figure 9(a)) decreases, and both heterogeneities surface (Figure 9(b)) and heterogeneities average area (Figure 9(c)) increases. For polymers blends based on $P[(S)_{96-co-(S-MOM-C_9F_{19})_4}] / PS$ and $P[(S)_{63-co-(S-MOM-C_9F_{19})_{37}}]$ discontinuous submicro-metric heterogeneities ($< 1 \mu m^2/Nb$ (Figure 9(c)) and continuous micro-metric heterogeneities ($> 1 \mu m^2/Nb$ (Figure 9(c)) are observed at low and high fluorine content, respectively. In contrast, $P[(S)_{81-co-(S-MOM-C_9F_{19})_{19}}]$ shows discontinuous phases independently of fluorine content, more numerous heterogeneities (Figure 9(a)), an order of magnitude lower heterogeneities surface (Figure 9(b)) and weak dependence of heterogeneities average area with fluorine content (Figure 9(c)). These observations are consistent with DSC analyses performed on polymers blends (not presented here) and the homogenous microstructure of $P[(S)_{81-co-(S-MOM-C_9F_{19})_{19}}]$.



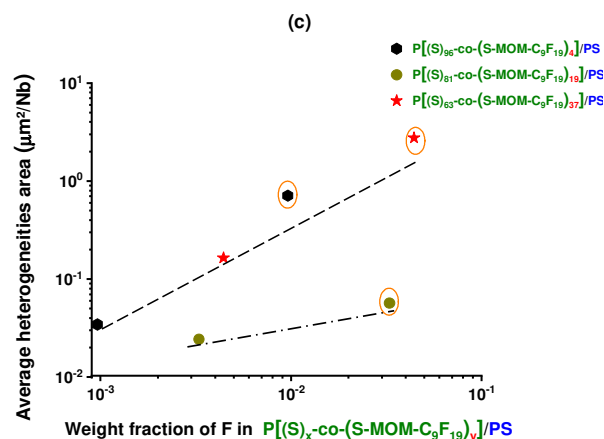
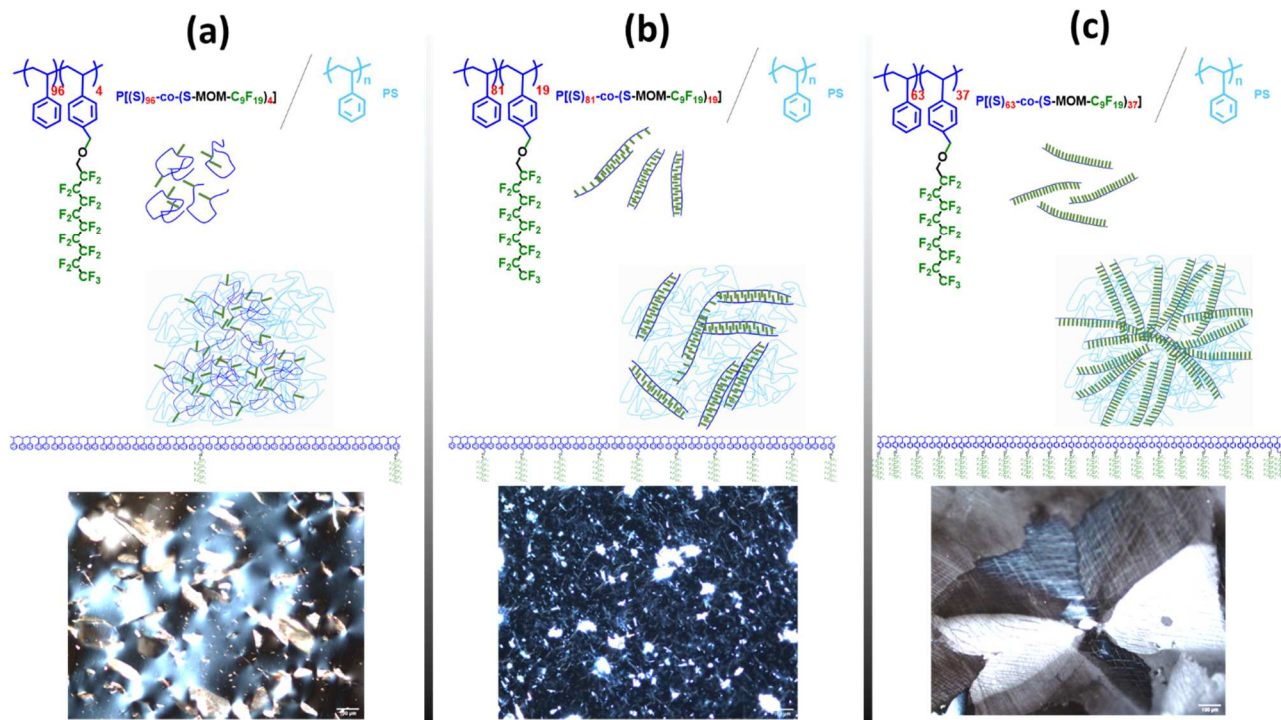


Figure 9. Quantification of (a) amount of heterogeneities (b) total heterogeneities area and (c) average heterogeneities area (heterogeneities area/ amount of heterogeneities) versus weight fraction of fluorine in $P[(S)_x\text{-co-(S-MOM-C}_9\text{F}_{19})_y]/\text{PS}$ blends. Surround points (corresponding to additives/PS 10 wt.%) are chosen for studying molecular structure-microstructure-miscibility with PS

II.1.4. Relationship molecular structure-microstructure-miscibility with PS

The Scheme 4 summarizes the hypotheses developed from all the characterisations, i.e., i/ at a molecular scale by NMR spectroscopy (in solution) and X-ray diffraction (at the solid state) ii/ at micro/nano-scale microstructure by DSC and micron-scale by optical microscopy of $P[(S)_{96}\text{-co-(S-MOM-C}_9\text{F}_{19})_4]$, $P[(S)_{81}\text{-co-(S-MOM-C}_9\text{F}_{19})_{19}]$ and $P[(S)_{63}\text{-co-(S-MOM-C}_9\text{F}_{19})_{37}]$ (surround points in Figure 9). The singular properties of $P[(S)_{81}\text{-co-(S-MOM-C}_9\text{F}_{19})_{19}]$ could be explained by a specific arrangement between side chains linked to specific inter/intramolecular interactions. In fact, $P[(S)_{81}\text{-co-(S-MOM-C}_9\text{F}_{19})_{19}]$ corresponds statistically (and theoretically) to 1 fluorinated graft spaced by 4 to 5 styrene monomers (Table 1) which could be favorable for an interdigitated conformation (Scheme 4(b)).[37, 41, 42] The voluminous fluorinated graft and the hindering steric disadvantage this conformation for $P[(S)_{63}\text{-co-(S-MOM-C}_9\text{F}_{19})_{37}]$, where 1 fluorinated graft is spaced by 2-3 styrene monomers (Table 1). The very spaced functionalized monomer in $P[(S)_{96}\text{-co-(S-MOM-C}_9\text{F}_{19})_4]$ (23-24 styrene spacers (Table 1)) doesn't allow an interpenetrated configuration (Scheme 4(a)).[37, 42]



Scheme 4. Optical microscopy images of surround points in Figure 9 (a) $P[(S)_{96}\text{-co-(S-MOM-C}_9\text{F}_{19})_4]/\text{PS } 10.\text{wt.}\%$ (b) $P[(S)_{81}\text{-co-(S-MOM-C}_9\text{F}_{19})_{19}]/\text{PS } 10.\text{wt.}\%$ (c) $P[(S)_{63}\text{-co-(S-MOM-C}_9\text{F}_{19})_{37}]/\text{PS } 10.\text{wt.}\%$. The schemes illustrate the hypotheses on the chains conformations and segregation arrangements plausible assumed for $P[(S)_x\text{-co-(S-MOM-C}_9\text{F}_{19})_y]$ according to the chemical composition of grafted fluorinated chain and the previous analyses NMR and DSC.

II.1.5. Wettability characterizations

II.1.5.1. Characterizations of the hydrophobicity

Figure 10 shows contact angles between water and formulated polymer blends as a function of additive $P[(S)_x\text{-co-(S-MOM-C}_9\text{F}_{19})_y]$ content (Figure 10(a), (b) and (c)) and the equivalent of fluorine content (Figure 10(a'), (b') and (c')). For the additive $P[(S)_{96}\text{-co-(S-MOM-C}_9\text{F}_{19})_4]$ (Figure 10(a) and (a')), below 10 wt.% of additive (1 wt.% of fluorine) the contact angle of the polymer blends is comparable to that of polystyrene (around 90°) and it is quasi-independent with additive content. Above this threshold, the contact angle increases sharply (red zone). Similar behavior was highlighted for the additive $P[(S)_{63}\text{-co-(S-MOM-C}_9\text{F}_{19})_{37}]$ with a threshold at 1 wt.% (0.1 wt.% of fluorine) and an amplified enhancement of contact angle of polymer blends (red zone), for a similar content of additive in comparison with $P[(S)_{96}\text{-co-(S-MOM-C}_9\text{F}_{19})_4]$. For the same content in additive $P[(S)_x\text{-co-(S-MOM-C}_9\text{F}_{19})_y]$, whatever the additive can be, the detected wettability threshold seems to be shifted

towards the lower fraction of additive with the increase in the fluorine content. The increase in the wetting angle would not depend only on the total amount of fluorine as confirmed by the presentation of contact angle as a function of fluorine content (in Figure 10(a'), (b') and (c')). In contrast, the water contact angle with P[(S)_{81-co}-(S-MOM-C₉F₁₉)₁₉] increases gradually and monotonously with additive content and obey a pseudo-linear law.

The unmodified contact angles found for various fluorine content coupled with the existence of thresholds stipulates an additional contribution of other factors including morphology and topography linked to the fluorine content. The evidence of a threshold (for P[(S)_{96-co}-(S-MOM-C₉F₁₉)₄] and P[(S)_{63-co}-(S-MOM-C₉F₁₉)₃₇]) and single-mode behaviors (P[(S)_{81-co}-(S-MOM-C₉F₁₉)₁₉]) also suggests the possible effect of the variable distribution of fluorinated graft along of polystyrene backbone (Scheme 2) highlighted by ¹H-NMR (Figure 1), ¹⁹F-NMR (Figure 2), ¹³C-NMR (Figure 3).

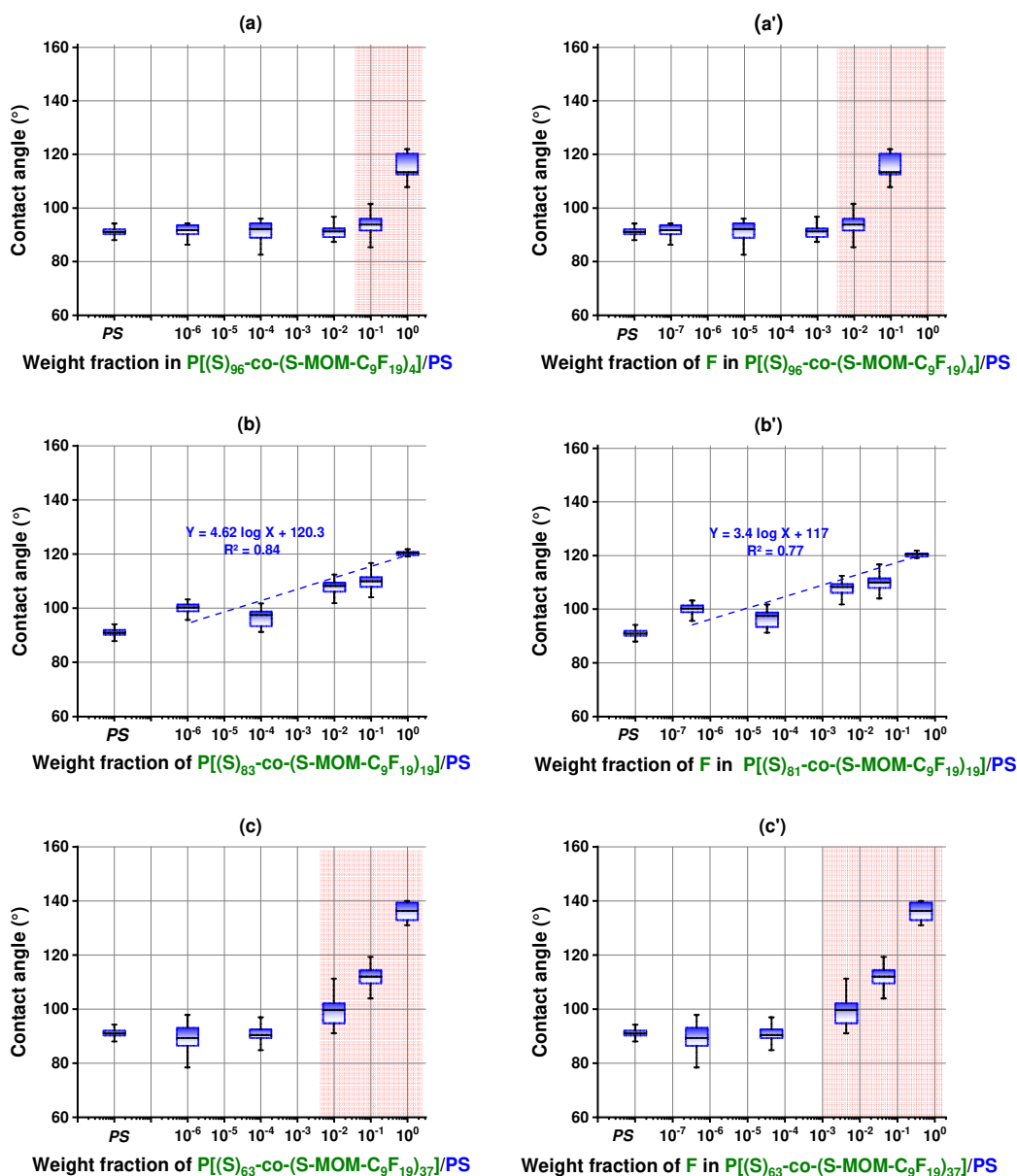


Figure 10. *Left: water-solid static contact angle versus $P[(S)_x-co-(S-MOM-C_9F_{19})_y]$ composition for (a) $P[(S)_{96}-co-(S-MOM-C_9F_{19})_4]/PS$, (b) $P[(S)_{81}-co-(S-MOM-C_9F_{19})_{19}]/PS$ and (c) $P[(S)_{63}-co-(S-MOM-C_9F_{19})_{37}]/PS$ Right: water-solid static contact angle versus fluorine composition in $P[(S)_x-co-(S-MOM-C_9F_{19})_y]/PS$ composition for (a') $P[(S)_{96}-co-(S-MOM-C_9F_{19})_4]/PS$, (b') $P[(S)_{81}-co-(S-MOM-C_9F_{19})_{19}]/PS$ and (c') $P[(S)_{63}-co-(S-MOM-C_9F_{19})_{37}]/PS$*

II.1.5.2. Characterizations of oleophobicity

Oleophobic properties were also investigated (Figure 11). Contact angles between silicon oil and formulated polymers blends as function of additive $P[(S)_x-co-(S-MOM-C_9F_{19})_y]$ content (Figure 11(a), (b) and (c)) in polymers blends and the equivalent of fluorine content (Figure 11 (a'), (b') and (c')). $P[(S)_{63}-co-(S-MOM-C_9F_{19})_{37}]$ and $P[(S)_{81}-co-(S-MOM-C_9F_{19})_{19}]$ exhibit bimodal threshold behaviors. At low content of additive $P[(S)_x-co-(S-$

MOM-C₉F₁₉)_y], oil-solid contact angle is independent with additive and fluorine. After the threshold, angle contact increases significantly (grey zone). In contrast, P[(S)₉₆-co-(S-MOM-C₉F₁₉)₄] seems not to have an effect on oil-solid contact angle because it contains an insufficient quantity of fluorine. Unlike the hydrophobic properties, similar oil-solid contact angles were obtained for similar fluorine content, whatever the additive can be. This suggests that the oleophobic properties are mainly dependent of quantity of fluorine and its contribution is overriding in relation to morphology and topography induced by the fluorine.

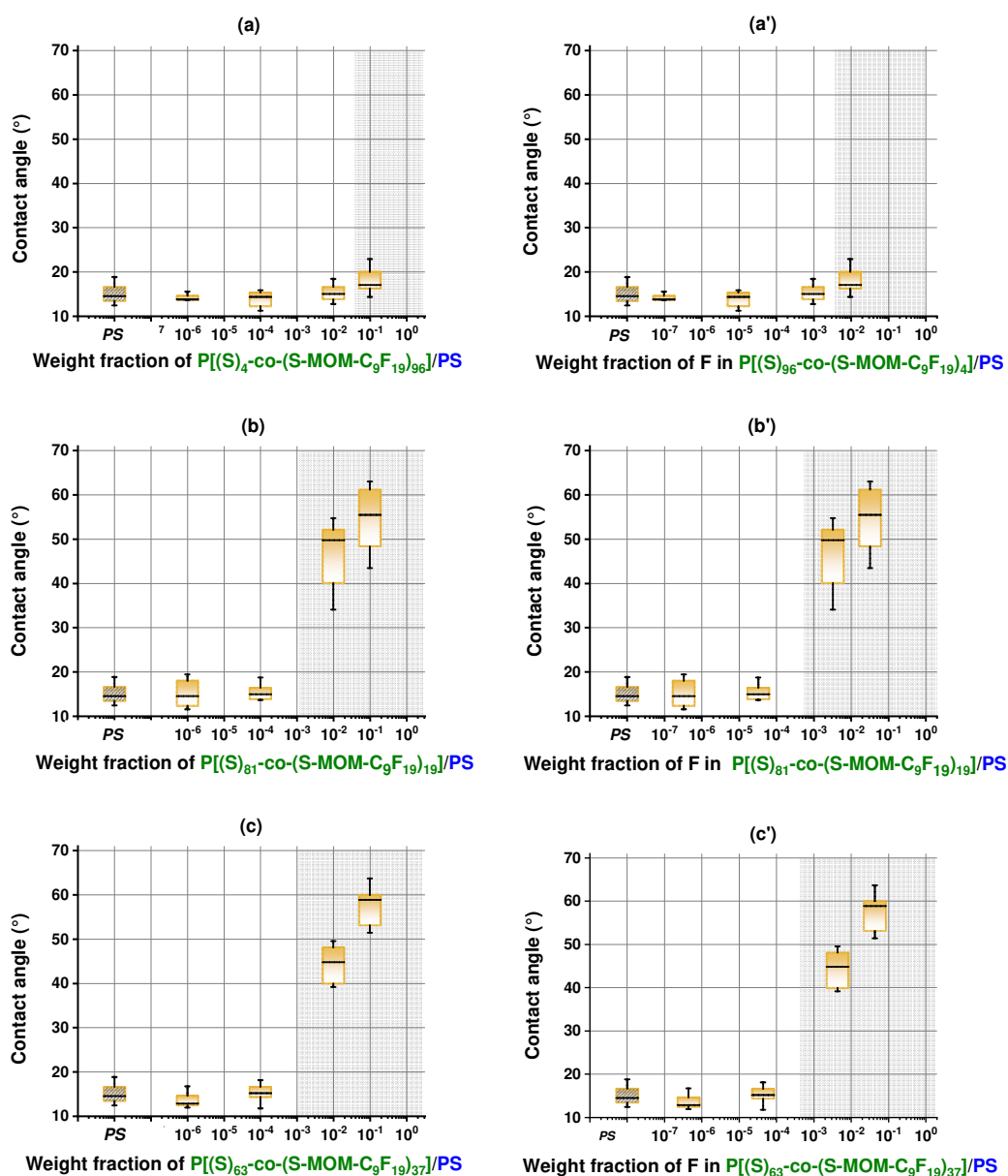


Figure 11. *Left:* oil-solid static contact angle versus $P[(S)_x\text{-co-(S-MOM-C}_9\text{F}_{19})_y]/PS$ composition for (a) $P[(S)_{96}\text{-co-(S-MOM-C}_9\text{F}_{19})_4]/PS$, (b) $P[(S)_{81}\text{-co-(S-MOM-C}_9\text{F}_{19})_{19}]/PS$ and (c) $P[(S)_{63}\text{-co-(S-MOM-C}_9\text{F}_{19})_{37}]/PS$ *Right:* oil-solid static contact angle versus fluorine composition in $P[(S)_x\text{-co-(S-MOM-C}_9\text{F}_{19})_y]/PS$ composition for (a') $P[(S)_{96}\text{-co-(S-MOM-C}_9\text{F}_{19})_4]/PS$, (b') $P[(S)_{81}\text{-co-(S-MOM-C}_9\text{F}_{19})_{19}]/PS$ and (c') $P[(S)_{63}\text{-co-(S-MOM-C}_9\text{F}_{19})_{37}]/PS$

III. Conclusion

In this work, semi-fluorinated random polystyrene copolymers were designed and developed as additives to improve hydrophobic and oleophobic surface properties of polystyrene. Two chemical synthesis strategies were tested. i) direct controlled radical copolymerization of styrene and perfluoromethylstyrene monomers, and ii) chemical modification via nucleophile substitution of chlorinated copolymers precursors synthesized by controlled radical copolymerization of styrene and 4-chloromethylstyrene monomers. The second route which allows better controls of the chemical structure and molar weight was adopted for the synthesis of various fluorinated additives with fluorinated monomer content of 4, 19 and 37 mol.% (11, 31, 45 wt.% of fluorine, respectively). All synthesis reactions were controlled by spectroscopic techniques: IR, $^1\text{H-NMR}$, $^{13}\text{C-NMR}$ and $^{19}\text{F-NMR}$. According to NMR analyses and microstructure characterizations by Differential Scanning Calorimetry, Optical Microscopy and X-ray diffraction, the additive based on 19 mol.% of fluorinated monomer exhibits particular properties and seems closer to a periodic/regular macromolecular conformation with a statistically alternation of 4-5 styrene between 2 fluorinated monomers. This specific conformation would promote an interpenetrating configuration and could explain the homogeneous morphology observed for this additive dispersed in a PS matrix, in comparison with copolymers based on 4 and 37 mol.% of fluorinated monomer.

The functionality of all synthesized copolymers was evaluated after their incorporation in a polystyrene matrix with various wt.% ranging from 100 ppm to 100% via a solvent process. The effects of nature and content of additive on hydrophobic and oleophobic surface properties were in particular investigated. For all additives, the more the additive content increases more, the surface properties are improved, obeying a threshold behavior for 4 and 37 mol.% and a quasi-linear behavior for 19 mol.%.

Finally, it was evidenced that the surface properties improvement results from both the presence of a minima percentage of fluorine in the polymers blends and its consequence on the morphology. The additive based on 19 mol.% of fluorinated monomer has a homogeneous morphology, independently of its content in polymers blends, allowing the achievement of higher contact angles even with very low percentages of additive. Beside the beneficial effects of this optimal additive on the surface properties of polystyrene, the effects on the rheological behavior during the industrial melt-processing including hot-embossing, extrusion or injection molding processes are expected.

IV. References

- [1] Y.J. Zhao, Z.B. Zhang, Y. Liu, J.H. Wang, J.L. Teng, L.S. Wu, Y.L. Zhang, The Principle and the Application of Self-cleaning Anti-pollution Coating in Power System, IOP Conference Series: Materials Science and Engineering 269 (2017) 012044.
- [2] S.S. Latthe, R.S. Sutar, V.S. Kodag, A.K. Bhosale, A.M. Kumar, K. Kumar Sadasivuni, R. Xing, S. Liu, Self – cleaning superhydrophobic coatings: Potential industrial applications, Progress in Organic Coatings 128 (2019) 52-58.
- [3] W. Zou, Z. Fan, S. Zhai, S. Wang, B. Xu, Z. Cai, A multifunctional antifog, antifrost, and self-cleaning zwitterionic polymer coating based on poly(SBMA-co-AA), Journal of Coatings Technology and Research 17(3) (2020) 765-776.
- [4] Z. Yang, L. Wang, W. Sun, S. Li, T. Zhu, W. Liu, G. Liu, Superhydrophobic epoxy coating modified by fluorographene used for anti-corrosion and self-cleaning, Applied Surface Science 401 (2017) 146-155.
- [5] L. Shen, B. Wang, J. Wang, J. Fu, C. Picart, J. Ji, Asymmetric Free-Standing Film with Multifunctional Anti-Bacterial and Self-Cleaning Properties, ACS Applied Materials & Interfaces 4(9) (2012) 4476-4483.
- [6] E.J. Falde, S.T. Yohe, Y.L. Colson, M.W. Grinstaff, Superhydrophobic materials for biomedical applications, Biomaterials 104 (2016) 87-103.
- [7] Y. Li, J. Bi, S. Wang, T. Zhang, X. Xu, H. Wang, S. Cheng, B.W. Zhu, M. Tan, Bio-inspired Edible Superhydrophobic Interface for Reducing Residual Liquid Food, Journal of agricultural and food chemistry 66(9) (2018) 2143-2150.
- [8] X. Huang, N. Tepylo, V. Pommier-Budinger, M. Budinger, E. Bonaccorso, P. Villedieu, L. Bennani, A survey of icephobic coatings and their potential use in a hybrid coating/active ice protection system for aerospace applications, Progress in Aerospace Sciences 105 (2019) 74-97.
- [9] R.N. Wenzel, RESISTANCE OF SOLID SURFACES TO WETTING BY WATER, Industrial & Engineering Chemistry 28(8) (1936) 988-994.
- [10] R.N. Wenzel, Surface Roughness and Contact Angle, The Journal of Physical and Colloid Chemistry 53(9) (1949) 1466-1467.
- [11] A.B.D. Cassie, S. Baxter, Wettability of porous surfaces, Transactions of the Faraday Society 40(0) (1944) 546-551.
- [12] J. Kijlstra, K. Reihls, A. Klamt, Roughness and topology of ultra-hydrophobic surfaces, Colloids and Surfaces A: Physicochemical and Engineering Aspects 206(1) (2002) 521-529.
- [13] G. Heydari, E. Thormann, M. Järn, E. Tyrode, P.M. Claesson, Hydrophobic Surfaces: Topography Effects on Wetting by Supercooled Water and Freezing Delay, The Journal of Physical Chemistry C 117(42) (2013) 21752-21762.
- [14] N. Nuraje, W.S. Khan, Y. Lei, M. Ceylan, R. Asmatulu, Superhydrophobic electrospun nanofibers, Journal of Materials Chemistry A 1(6) (2013) 1929-1946.
- [15] X. Gong, S. He, Highly Durable Superhydrophobic Polydimethylsiloxane/Silica Nanocomposite Surfaces with Good Self-Cleaning Ability, ACS Omega 5(8) (2020) 4100-4108.
- [16] X.-F. Zhang, J.-P. Zhao, J.-M. Hu, Abrasion-Resistant, Hot Water-Repellent and Self-Cleaning Superhydrophobic Surfaces Fabricated by Electrophoresis of Nanoparticles in Electrodeposited Sol-Gel Films, Advanced Materials Interfaces 4(13) (2017) 1700177.
- [17] L.-K. Wu, J.-M. Hu, J.-Q. Zhang, One step sol-gel electrochemistry for the fabrication of superhydrophobic surfaces, Journal of Materials Chemistry A 1(46) (2013) 14471-14475.
- [18] K. Manoharan, S. Bhattacharya, Superhydrophobic surfaces review: Functional application, fabrication techniques and limitations, Journal of Micromanufacturing 2 (2019) 59 - 78.

- [19] S.J. Hardman, N. Muhamad-Sarih, H.J. Riggs, R.L. Thompson, J. Rigby, W.N.A. Bergius, L.R. Hutchings, Electrospinning Superhydrophobic Fibers Using Surface Segregating End-Functionalized Polymer Additives, *Macromolecules* 44(16) (2011) 6461-6470.
- [20] E.C. Achilleos, G. Georgiou, S.G. Hatzikiriakos, Role of processing aids in the extrusion of molten polymers, *Journal of Vinyl and Additive Technology* 8(1) (2004) 7-24.
- [21] K.B. Migler, C. Lavallée, M.P. Dillon, S.S. Woods, C.L. Gettinger, Visualizing the elimination of sharkskin through fluoropolymer additives: Coating and polymer–polymer slippage, *Journal of Rheology* 45(2) (2001) 565-581.
- [22] U.M. Attia, S. Marson, J.R. Alcock, Micro-injection moulding of polymer microfluidic devices, *Microfluid. Nanofluid.* 7(1) (2009) 1.
- [23] K. Matyjaszewski, B.E. Woodworth, X. Zhang, S.G. Gaynor, Z. Metzner, Simple and Efficient Synthesis of Various Alkoxyamines for Stable Free Radical Polymerization, *Macromolecules* 31(17) (1998) 5955-5957.
- [24] D.W. Smith, S.T. Iacono, S.S. Iyer, *Handbook of Fluoropolymer Science and Technology*, Wiley 2014.
- [25] L. Andruzzi, E. Chiellini, G. Galli, X. Li, S.H. Kang, C.K. Ober, Engineering low surface energy polymers through molecular design: synthetic routes to fluorinated polystyrene-based block copolymers, *Journal of Materials Chemistry* 12(6) (2002) 1684-1692.
- [26] A. Zaggia, L. Conte, G. Padoan, F. Ceretta, Synthesis and characterization of partially fluorinated ethers, *Journal of Fluorine Chemistry* 131(8) (2010) 844-851.
- [27] G.G. Hougham, P.E. Cassidy, K. Johns, T. Davidson, *Fluoropolymers 1: Synthesis*, Springer US 2006.
- [28] W. Chen, L. Xu, J. Xiao, Fluorous soluble polymer catalysts for the fluorous biphasic hydroformylation of olefins, *Chemical Communications* (10) (2000) 839-840.
- [29] J. Hopken, M. Moller, Low-surface-energy polystyrene, *Macromolecules* 25(5) (1992) 1461-1467.
- [30] T. Barman, H. Chen, J. Liu, G. Yang, W. Zhao, C. Peng, X. Hou, Synthesis and characterization of styrene-based polyfluoroacrylate film for hydrophobic/icephobic applications, *Thin Solid Films* 687 (2019) 137462.
- [31] J. Alex, J. Ulbrich, M. Rosales-Guzmán, C. Weber, U.S. Schubert, C. Guerrero-Sanchez, Kinetic investigations on homo- and co-polymerizations of pentafluorophenyl (meth)acrylates, *European Polymer Journal* 143 (2021) 110175.
- [32] A. Hillmyer Marc, P. Lodge Timothy, Synthesis and self-assembly of fluorinated block copolymers, *Journal of Polymer Science Part A: Polymer Chemistry* 40(1) (2001) 1-8.
- [33] A. Nourdine, L. Perrin, R.d. Bettignies, S. Guillerez, L. Flandin, N. Alberola, Synthesis and characterization of fullerene based systems for photovoltaic applications: Evidence for percolation threshold, *Polymer* 52(26) (2011) 6066-6073.
- [34] B.S. Chang, L. Ma, M. He, T. Xu, NMR Studies of Block Copolymer-Based Supramolecules in Solution, *ACS Macro Letters* 9(7) (2020) 1060-1066.
- [35] K. Nishimori, E. Cazares-Cortes, J.-M. Guigner, F. Tournilhac, M. Ouchi, Physical gelation of AB-alternating copolymers made of vinyl phenol and maleimide units: cooperation between precisely incorporated phenol and long alkyl pendant groups, *Polymer Chemistry* 10(18) (2019) 2327-2336.
- [36] Nonappa, E. Kolehmainen, Solid state NMR studies of gels derived from low molecular mass gelators, *Soft Matter* 12(28) (2016) 6015-6026.
- [37] L. Arnedo-Sánchez, Nonappa, S. Bhowmik, S. Hietala, R. Puttreddy, M. Lahtinen, L. De Cola, K. Rissanen, Rapid self-healing and anion selectivity in metallosupramolecular gels assisted by fluorine–fluorine interactions, *Dalton Transactions* 46(22) (2017) 7309-7316.
- [38] M. Kobayashi, I. Ando, T. Ishii, S. Amiya, Structural study of poly(vinyl alcohol) in the gel state by high-resolution solid-state ¹³C NMR spectroscopy, *Macromolecules* 28(19) (1995) 6677-6679.
- [39] E.N. Brown, P.J. Rae, D.M. Dattelbaum, B. Clausen, D.W. Brown, In-situ Measurement of Crystalline Lattice Strains in Polytetrafluoroethylene, *Experimental Mechanics* 48(1) (2008) 119-131.
- [40] K. Honda, M. Morita, H. Otsuka, A. Takahara, Molecular Aggregation Structure and Surface Properties of Poly(fluoroalkyl acrylate) Thin Films, *Macromolecules* 38(13) (2005) 5699-5705.

- [41] S. Pensec, F.-G. Tournilhac, P. Bassoul, C. Durliat, Synthesis and Structural Studies of Polyphilic Mesogens with Central or Terminal Perfluoroalkyl Chains, *The Journal of Physical Chemistry B* 102(1) (1998) 52-60.
- [42] K. Inomata, E. Nakanishi, Y. Sakane, M. Koike, T. Nose, Side-chain crystallization behavior of graft copolymers consisting of amorphous main chain and crystalline side chains: Poly(methyl methacrylate)-graft-poly(ethylene glycol) and poly(methyl acrylate)-graft-poly(ethylene glycol), *Journal of Polymer Science Part B: Polymer Physics* 43(1) (2005) 79-86.
- [43] G. De Crevoisier, P. Fabre, L. Leibler, S. Tencé-Girault, J.M. Corpart, Structure of Fluorinated Side-Chain Smectic Copolymers: Role of the Copolymerization Statistics, *Macromolecules* 35(10) (2002) 3880-3888.
- [44] R. Sarkar, E.B. Gowd, S. Ramakrishnan, Precise control of grafting density in periodically grafted amphiphilic copolymers: an alternate strategy to fine-tune the lamellar spacing in the sub-10 nm regime, *Polymer Chemistry* 11(25) (2020) 4143-4154.
- [45] S. Chanda, S. Ramakrishnan, Controlling Interlamellar Spacing in Periodically Grafted Amphiphilic Copolymers, *Macromolecules* 49(9) (2016) 3254-3263.
- [46] G.O. Orodepo, E.B. Gowd, S. Ramakrishnan, Main-chain liquid crystalline polymers bearing periodically grafted folding elements, *Polymer Chemistry* 12(7) (2021) 1050-1059.

Acknowledgments:

The authors thank Laure Cointeaux and Vincent Martin from LEPMI for their valuable help and the provision of the equipment/accessories required for the NMR and SEC analyses, respectively. Thierry Encinas from the CMTC (Consortium des Moyens Technologiques Communs) is acknowledged for the X-Ray diffraction measurements. Some of this work has been conducted thanks to the support of the Auvergne Rhone Alpes region through the grant N°20-009580-01 given in the framework of the Pack Ambition Recherche 2020 - Projet EFFISURF. The ANRT (Association Nationale de la Recherche et de la Technologie) is also acknowledged for its contribution to the funding of a PhD thesis. Mrs. Sandrine LEBIGRE (IPC, Bellignat) is particularly acknowledged for her advices. The authors thank also Yannick Molméret and Dominique Meillassoux from IPC (Centre Technique Industriel de la Plasturgie et des Composites) for their fruitful scientific discussions.

Conflict of interest

The authors declare that they have no conflict of interest.